IEEE Access
Multidisciplinary | Rapid Review | Open Access Journal

Received January 18, 2019, accepted February 5, 2019, date of publication February 25, 2019, date of current version March 12, 2019.

Digital Object Identifier 10.1109/ACCESS.2019.2901691

A Framework for Image Denoising Using First and Second Order Fractional Overlapping Group Sparsity (HF-OLGS) Regularizer

AHLAD KUMAR, M. OMAIR AHMAD, (Fellow, IEEE), AND M. N. S. SWAMY, (Fellow, IEEE)
Department of Electrical and Computer Engineering, Concordia University, Montreal, QC H3G 1M8, Canada

Corresponding author: M. N. S. Swamy (swamy@ece.concordia.ca)

This work was supported in part by the Horizon Postdoctoral Fellowship and Research Chair Programs, Concordia University, in part by the Natural Sciences and Engineering Research Council (NSERC), Canada, and in part by the Regroupement Strategique en Microelectronique du Quebec (ReSMiQ).

ABSTRACT Denoising images subjected to Gaussian and Poisson noise has attracted attention in many areas of image processing. This paper introduces an image denoising framework using higher order fractional overlapping group sparsity prior to sparser image representation constraint. The proposed prior has a capability of avoiding staircase effects in both edges and oscillatory patterns (textures). We adopt the alternating direction method of multipliers for optimizing the proposed objective function by converting it into a constrained optimization problem using variable splitting approach. Finally, we conduct experiments on various degraded images and compare our results with those of several state-of-the-art methods. The numerical results show that the proposed fractional order image denoising framework improves the peak signal to noise ratio of an image by preserving the textures and eliminating the staircases effects. This leads to visually pleasant restored images which exhibit a higher value of Structural SIMilarity score when compared to that of other methods.

INDEX TERMS Image denoising, fractional-order, Gaussian and Poisson noise, overlapping group sparsity, alternating direction method of multipliers.

I. INTRODUCTION

Digital images play an important role in our lives as they are used in a variety of applications such as television, astronomy and traffic monitoring systems. The techniques involved in acquiring these images introduce various types of noise and artifacts. Preserving the details of an image and removing unwanted random noise as much as possible is the goal of image denoising. Moreover, the noisy image produces undesirable visual quality and reduces the visibility of low contrast images. Hence the task of image denoising in digital applications is to enhance and recover finer details that are present in the data.

Images are often degraded due to Gaussian and Poisson noise during the process of acquisition or transmission. As a result, it is one of the most important issues which needs to be resolved for its proper use in the field of computer vision and graphics community. The degradation model in the case of Gaussian noise is defined by the following linear space invariant system:

$$g = Hu + n \tag{1}$$

while in the case of Poisson noise, the model can be statistically modelled as

$$g = Poiss(Hu) \tag{2}$$

where g is the obtained degraded image, H denotes the blur kernel commonly known as the point spread function (PSF), u is the desired original image, n is the zero mean Gaussian white noise and $Poiss(v)$ is an independent and identically distributed (iid) Poisson random vector with the Poisson parameter v.

The aim of image restoration is to recover u from g and is often known to be a classic ill-posed inverse problem, which is highly sensitive to noise degradation even if the blur kernel H is known exactly. In order to solve this ill-posed nature of the problem, one resorts to solving the following

The associate editor coordinating the review of this manuscript and approving it for publication was Jeon Gwanggil.

2169-3536 © 2019 IEEE. Translations and content mining are permitted for academic research only.
Personal use is also permitted, but republication/redistribution requires IEEE permission.
See http://www.ieee.org/publications_standards/publications/rights/index.html for more information.

minimization objective

$$\min_{u} \{E(u, g) + \lambda R(u)\} \tag{3}$$

where E is the data fidelity term that measures how close the estimated u is to the observation g, while R is the regularization prior and λ is the regularization parameter that balances the two terms. Various priors have been developed in the literature to regularize the ill-posed problem in (3), such as the zero-mean mixture-of-Gaussian model [1], sparse approximation [2], hyper-Laplacian [3] and normalized sparisity measure [4]. There are several methods for denoising the image, but our focus in this paper is on image denoising framework that involves total variation (TV) and its variants. The Rudin-Osher-Fatemi (ROF) model [5] is one of the standard ways of denoising the images and provides a good trade-off between edge preservation and noise removal. However, this method tends to produce staircase effects at the sharp edges of an image. In order to alleviate this issue, several solutions have been proposed in the literature. One of the solutions is to replace the traditional total variation (TV) by a higher-order TV norm that results in a piecewise linear solution which better fits the smooth intensity changes. Chan *et al.* [6] proposed an improved higher-order TV model by adding a fourth order term to Euler Lagrange (EL) equations for the TV model. Lysaker and Tai [7] proposed a method of combining fourth order partial differential equation (PDE) with TV filter. The combination helps to preserve the edges and avoid staircase effects created in smooth regions. Papafitsoros and Schönlieb [8] proposed a higher order extension of ROF functional by adding a non-smooth second order regularizer, and employed split Bregman method to solve the corresponding denoising framework. Noise removal using a fourth order partial differential equation with its application to magnetic resonance images is proposed in [9]. The use of nonlocal TV model proves to be an effective image prior for overcoming the staircase effects in noisy images [10].

The methods proposed for additive Gaussian noise are not directly applicable to Poisson noise due to its image dependent nature as given in (2). Moreover, the problem of denoising images degraded due to Poisson noise is gaining attention in recent years. Liu *et al.* [11] proposed a higher-order TV norm along with traditional TV to balance the edge and smoothness regions of the image degraded due to Poisson noise. Zhou and Li [12] proposed the use of fourth order partial differential equations for Poisson noise removal. A new regularizer prior known as the total generalized variation (TGV) is proposed by Bredies *et al.* [13]. The proposed functional regularizes on different regularity levels and does not produce any staircasing effect. An iterative reweighed TGV is proposed later for effective Poisson noise removal [14]. Shi *et al.* [15] proposed a Poisson based image deblurring using non-local total variational term. Here, the concept of framelet regularizer is proposed to enhance the sparsity of the images. The overall optimization problem is solved using split Bregman method. Landi and Piccolomini [16] proposed an iterative method for non-negatively constrained TV denoising for medical images corrupted by Poisson noise and the effectiveness of the method is evaluated on real and synthetic datasets. A primal dual method for deblurring the images degraded due to Poisson noise is formulated having demonstrated the robust convergence properties [17].

Recently, fractional order total variation models have been proposed in the area of image denoising [18]–[20], image inpainting [21] and super-resolution [22]. Moreover, the use of fractional order partial differential equations applied to the problem of image denoising is also gaining popularity. Bai and Feng [23] solved the problem of image denoising framework using nonlinear anisotropic fractional diffusion equation which is based on Euler-Lagrange formulation. Although total variation (TV)-based methods are effective in preserving edges and details in an image, they tend to produce staircase effects. To solve this problem, Ding *et al.* [24] proposed a new convex model based on TV with overalpping group sparisty for restoring images degraded due to blur but Cauchy noise. A new convex model has been proposed by Zhao *et al.* [25] for restoring blurred images degraded by multiplicative noise. The task of image denoising has widespread application in the field of medical imaging also [26]–[30]

Another way of denoising is first to decompose an image into structural (edges) and texture (oscillatory) parts and then to denoise each part. The structural part is represented by a piecewise smooth function, while the texture components by an oscillatory function. Such a decomposition has been adopted in various variational models and wavelet analysis [31]–[33]. Chen and Cheng [34] proposed a novel hybrid variational model for deconvolving Poissonian image by representing images as a composition of a structural part and a detailed part. The structural part is characterized using total variation, while the detailed part is characterized using sparse representation over the wavelet basis. A spatially adapted fractional order TV has been introduced for different texture regions in [35]. The results are promising, but finding the texture map is not an easy task. Providing regularization with different orders make use of many neighborhood cells that can result in undesired artifacts, especially near the boundaries. Fractional order derivatives are also suitable for denoising texture present in an image [36], [37]. A linear fractional integro-differential equation to control the diffusion effect in image enhancement is proposed by Cuesta *et al.* [38]. A novel fractional-order differentiation model for low dose medical images is proposed in [39]. This model is basically a weighted combination of fractional-order TV model and fractional-order Perona-Malik (PM) model. This is done in order to take advantage of TV, PM and fractional-order models.

Liu *et al.* [40] proposed an effective regularization prior comprising of overlapping group sparsity for image restoration. This method of imposing the prior proved to be an effective way of reducing the staircase effects in the structural (edges) component of an image. However, it is not

effective in restoring the texture components present in an image due the presence of staircase effects. It has been observed that fractional order derivatives are effective in restoring the texture components of an image [20]. In our present paper, we have considered an extension of Liu's work by introducing higher order fractional based overlapping group sparsity regularizers (HF-OLGS) to overcome this deficiency of Liu's method. Here, the denoising framework is solved using well known optimization framework, the alternating direction method of multipliers (ADMM) [41].

To summarize, the main contributions of this work are as follows: (1) Image denoising model dealing with Gaussian and Poisson noise is proposed using higher order fractional based overlapping group sparsity (HF-OLGS) prior (2) The proposed framework is capable of simultaneously preserving the sharpness of the image edges and reducing the undesirable staircase effects in the oscillating patterns that correspond to the texture area in an image.

The rest of this paper is organized as follows. In Section II, a brief discussion of the preliminaries which includes overlapping group sparsity, fractional-order and ADMM is discussed. Sections III and IV discuss the proposed model and the image denoising framework respectively. Experimental results are given in Section V. Finally, conclusions are given in Section VI.

II. PRELIMINARIES

This section discusses some of the mathematical preliminaries needed to understand the motivation for the proposed image denoising framework. It starts with a discussion of overlapping group sparsity followed by the concepts of fractional calculus and its applications in image processing. Lastly, a brief summary of the famous optimization framework known as alternating direction method of multipliers (ADMM) is discussed which will be used in our proposed work.

A. OVERLAPPING GROUP SPARSITY (OLGS)

For one dimensional signal processing, the concept of overlapping group sparsity (OLGS) was first introduced in [42] for the case of signal denoising. The concept of overlapping group structure as signal prior was introduced in alleviating the staircase effects when compared to standard total variation (TV) denoising. In [40], a K-point group of the vector $l \in R^n$ has been defined as

$$l_{i,K} = [l(i), l(i+1), \ldots, l(i+K-1)] \in R^K \tag{4}$$

It can be observed that $l_{i,K}$ can be seen as a block of K contiguous sample of l starting at index i. Group sparsity regularizer [43], [44] in one dimensional case is defined as

$$\eta(l) = \sum_{i=1}^{n} \left\| l_{i,K} \right\|_2 \tag{5}$$

where the group size is denoted by K. For two-dimensional case, a $K \times K$ point group of the image u of size $N \times M$ is defined as

$$\tilde{u}_{i,j,K} = \begin{bmatrix} u_{i-m_1,j-m_1} & u_{i-m_1,j-m_1+1} & \cdots & u_{i-m_1,j+m_2} \\ u_{i-m_1+1,j-m_1} & u_{i-m_1+1,j-m_1+1} & \cdots & u_{i-m_1+1,j+m_2} \\ \vdots & \vdots & \ddots & \vdots \\ u_{i+m_2,j-m_1} & u_{i+m_2,j-m_1+1} & \cdots & u_{i+m_2,j+m_2} \end{bmatrix} \tag{6}$$

with $m_1 = \left\lfloor \frac{K-1}{2} \right\rfloor$ and $m_2 = \left\lfloor \frac{K}{2} \right\rfloor$. Here, $\lfloor x \rfloor$ denotes the greatest integer not greater than x. The overlapping group sparsity (OLGS) functional for a two-dimensional array is defined as

$$\phi(u) = \sum_{i,j=1}^{n} \left\| u_{i,j,K}(:) \right\|_2 \tag{7}$$

where $u_{i,K}(:)$ is a vector obtained by stacking the columns of matrix $\tilde{u}_{i,K}(:)$. The regularization term $\phi(u)$ [40] based on the image gradients in vertical and horizontal directions is given as

$$\phi(u) = \phi(D_x u) + \phi(D_y u) \tag{8}$$

where D is the discrete gradient operator defined as

$$(D_x(u))_{i,j} = \begin{cases} u_{i+1,j} - u_{i,j}, & \text{if} \quad i < M \\ u_{1,j} - u_{M,j}, & \text{if} \quad i = M \end{cases}$$

$$(D_y(u))_{i,j} = \begin{cases} u_{i,j+1} - u_{i,j}, & \text{if} \quad j < N \\ u_{i,1} - u_{i,N}, & \text{if} \quad j = N \end{cases}$$

B. FRACTIONAL ORDER PROCESSING

As the generalization of the integer-order derivative, this paper utilizes the concept of fractional order derivative for the purpose of image denoising. The fractional order derivatives to be used in the regularizer of the proposed denoising framework (Sec. IV) are defined as

$$D_x^\alpha u(i,j) \approx \sum_{k=0}^{K} \Psi_\alpha(k) u(i-k,j), \qquad i = 1, \ldots, M \quad j = 1, \ldots, N$$

$$D_y^\alpha u(i,j) \approx \sum_{k=0}^{K} \Psi_\alpha(k) u(i,j-k), \qquad i = 1, \ldots, M \quad j = 1, \ldots, N \tag{9}$$

where $\Psi_\alpha(k) = (-1)^k \ \Gamma(\alpha+1)/[k! \ \Gamma(\alpha-k+1)]$. Further details regarding the properties of the fractional-order total variation can be found in [41] and [46]. Here, D_x^α and D_y^α are the discrete fractional-order derivatives of an image u of size $M \times N$ at (i,j) in the vertical and horizontal directions respectively. The complex conjugate operation corresponding to (9) is defined as

$$(D_x^\alpha)^* u(i,j) \approx \sum_{k=0}^{K} \Psi_\alpha(k) u(i+k,j), \qquad i = 1, \ldots, M \quad j = 1, \ldots, N$$

$$(D_y^{\alpha})^* u(i,j) \approx \sum_{k=0}^{K} \Psi_{\alpha}(k) u(i, j+k), \quad i = 1, \ldots, M \quad j = 1, \ldots, N \tag{10}$$

Here $*$ denotes the complex conjugate operation and $(D_x^{\alpha})^*$,$(D_y^{\alpha})^*$ are the complex conjugate operators corresponding to (D_x^{α}) and (D_y^{α}) respectively. The parameter K given in (9)-(10) is a sufficiently large integer. Further, the magnitude of $\phi_{\alpha}(k)$ tends to become zero very fast as $k \to \infty$. Hence, in this manuscript the value of K is taken as 20 [19], [35], [45].

C. ADMM

A very powerful algorithm that is very well suited for convex optimization and finds extensive role in the area of applied statistics and machine learning is known as alternating direction method of multipliers (ADMM) [41]. It is an efficient and effective technique for solving multi-parameter constrained optimization problems, hence it will be used for solving the proposed optimization framework discussed in Sec. IV. The algorithm solves problems in the form as follows:

$$\begin{aligned} &\min_{x,y} f(x) + e(y), \\ &\text{s.t. } Ax + By = b \end{aligned} \tag{11}$$

where f and e are convex functions. Further, A and B are the two operators. With the Lagrangian multiplier λ to the linear constraint stated in problem (11), the augmented Lagrangian function [46] for the problem (11) is defined as $L(x, y, \lambda) = f(x) + e(y) + \lambda^T (Ax + By - b) + \frac{\sigma}{2} \|Ax + By - b\|_2^2$, where σ is the penalty parameter for the linear constraint. According to the concept of ADMM, the optimal solution is obtained by finding the saddle point of $L(x, y, \lambda)$ using the alternating minimization scheme, such as keeping x and λ constant when minimizing L with respect to y. We obtain the following ADMM iterative minimization algorithm

$$\begin{cases} x^{i+1} = \underset{x}{\operatorname{argmin}}\, L(x, y^i, \lambda^i) \\ y^{i+1} = \underset{y}{\operatorname{argmin}}\, L(x^{i+1}, y, \lambda^i) \\ \lambda^{i+1} = \lambda^i - \sigma(Ax^{i+1} + By^{i+1} - b) \\ i = i + 1; \end{cases} \tag{12}$$

III. PROPOSED HIGHER ORDER FRACTIONAL OVERLAPPING GROUP SPARISTY (HF-OLGS) REGULARIZER

In this paper, the proposed regularizer R termed as (HF-OLGS) used for the image denoising framework is chosen to be the sum of the fractional based overlapping group sparsity (F-OLGS) and the second order version of the F-OLGS, weighted using two positive parameters β_1 and β_2 respectively, i.e.,

$$\begin{aligned} R_{\beta_1,\beta_2,\alpha}(u) = \beta_1 \left[\phi(D_x^{\alpha} u) + \phi(D_y^{\alpha} u) \right] \\ + \beta_2 \left[\phi(D_{xx}^{\alpha} u) + \phi(D_{yy}^{\alpha} u) + 2\phi(D_{xy}^{\alpha} u) \right] \end{aligned} \tag{13}$$

Here, D_x^{α}, D_y^{α}, D_{xx}^{α}, D_{yy}^{α} and D_{xy}^{α} the fractional operators discussed in Section II-B and $\phi(.)$ is the OLGS operator discussed in Section II-A.

To evaluate the performance of the regularizer proposed in (13), we consider its 1D version as

$$R_{\beta_1,\beta_2,\alpha}(u) = \beta_1 \left[\phi(D_x^{\alpha} u) \right] + \beta_2 \left[\phi(D_{xx}^{\alpha} u) \right] \tag{14}$$

The motivation of incorporating the second order term in the F-OLGS regularizer in (14) is to simultaneously preserve the sharpness of the image edges and further reduce the undesirable staircase effects in the oscillating patterns which correspond to the texture area in the image. We now consider two test signals to prove the effectiveness of the regularizer in (14). The first signal $u(n)$ is selected in such a way that it represents a combination of the edge and texture (*Edges* + *Texture*) profiles, as shown in Fig.1(a). The corresponding noisy observation $g(n)$ is plotted in Fig.1(b). The restored signals $\widehat{u}(n)$ obtained using TV, OLGS, first and second order derivatives (H-OLGS) and the proposed HF-OLGS regularizers, are shown in Figs.1(c),(d),(e) and (f), respectively. It can be observed from Fig.1(c) that the conventional TV regularizer creates staircase artifacts in both the edge and texture profiles. However, the OLGS regularizer effectively reduces the staircase effects in the edge profile region, but its performance in the corresponding texture profile region still contains staircase effects as seen from Fig.1(d). This staircase phenomenon found in texture region is reduced using H-OLGS regularizer as seen from Fig.1(e), but it results in tapering off of the peaks of the signal in the texture part. It can be observed from Fig. 1(f) that by using the proposed regularizer, both the edge and texture profiles are restored effectively with less staircase effects compared to that using other regularizers. Also, we do not observe any tapering phenomenon using our proposed regularizer. The RMSE values for the corresponding restored signals shown in Figs.1(c)-(f) are 0.2868, 0.2644, 0.2412 and 0.2354, respectively, indicating the lowest RMSE value for the proposed HF-OLGS regularizer. Next, a second test signal, a combination of two different texture profiles (*Texture* 1 + *Texture* 2), shown in Fig. 2(a) is now considered. It can be observed that for these two different texture profiles, both TV and OLGS exhibit staircase effects, as seen from Fig. 2(c) and (d). But, the staircase effects in OLGS are slightly less than that from using TV, resulting in RMSE values of 0.4223 and 0.3567, respectively. With the use of H-OLGS regularizer, the staircase effect is reduced in the two texture profiles, as seen from Fig. 2(e). However, the reconstruction at the lower part of *Texture* 2 signal suffers from some noisy component being present. But, with the use of the proposed HF-OLGS regularizer, the staircase effects are very minimal compared to that using TV, OLGS or H-OLGS regularizer, as seen from Fig. 2(f). Further, the reconstruction quality of the restored signal is good, as seen from the corresponding RMSE value for the restored signal, which is 0.2725. Thus, the effectiveness of the proposed regularizer in terms of its ability in reducing the staircase effects for both the edge and texture regions is

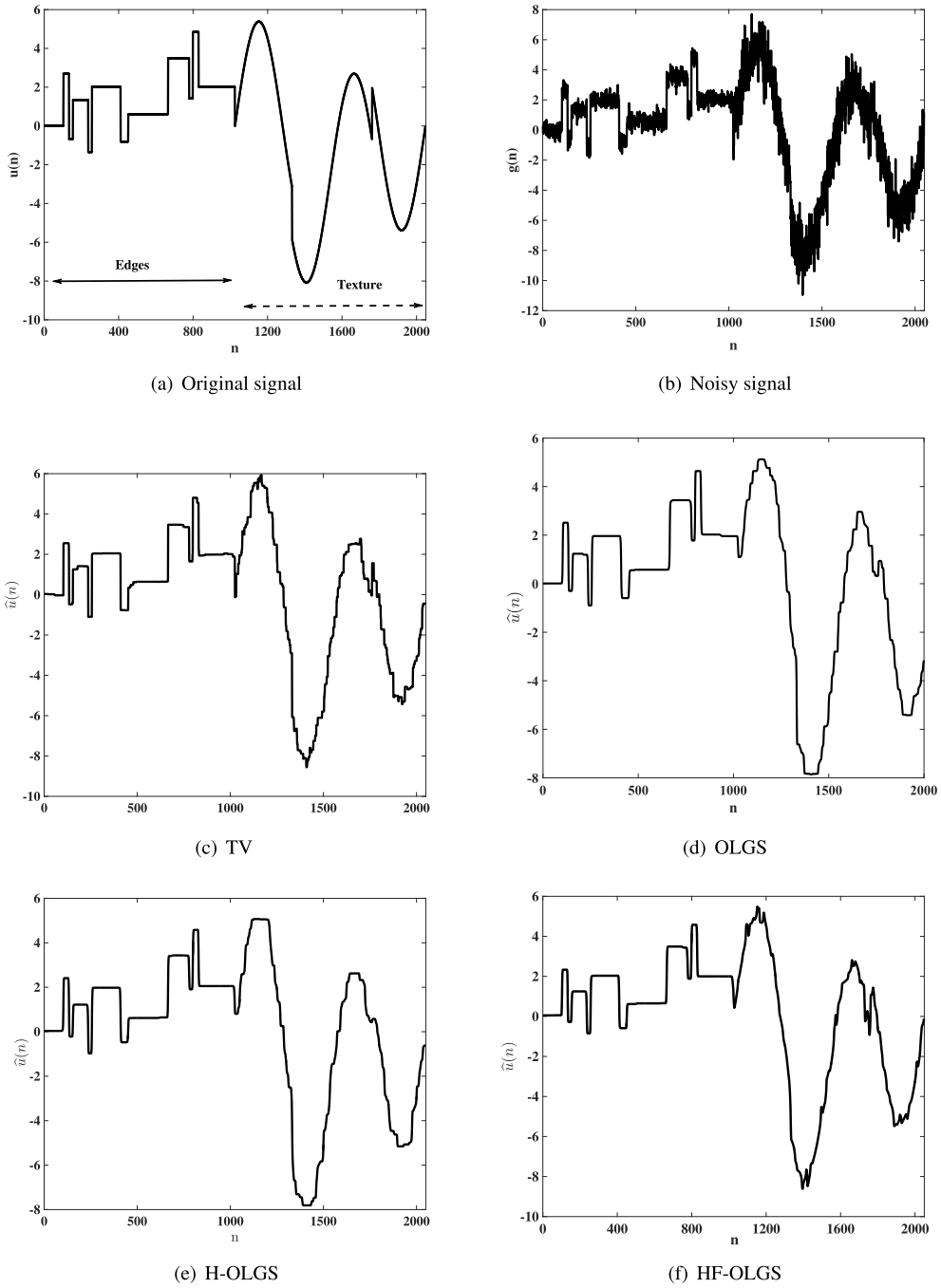

(a) Original signal (b) Noisy signal

(c) TV (d) OLGS

(e) H-OLGS (f) HF-OLGS

FIGURE 1. Restoration of test signal (*Edge* + *Texture*) using TV, OLGS, H-OLGS and HF-OLGS regularizers. (a) Original signal. (b) Noisy signal. (c) TV. (d) OLGS. (e) H-OLGS. (f) HF-OLGS.

demonstrated in this section using one dimensional signals. In the next section, we discuss the proposed image denoising framework using the 2D version of the regularizer given in (14).

IV. PROPOSED IMAGE DENOISING FRAMEWORK

Total variation is one of the standard techniques for removing the noise effectively from an image by suppressing the ringing effects and preserving the sharp edges. However, it still has a shortcoming of creating staircase effects which are not desirable. In order to take advantage of TV regularization and relieve from staircase effects, we propose a higher order fractional overlapping group sparsity (Sec. III)-based image denoising framework defined as

$$\min_{u} \Big\{ Z = E(u,g) + \beta_1 \Big[\phi(D_x^{\alpha}u) + \phi(D_y^{\alpha}u) \Big] + \beta_2 \Big[\phi(D_{xx}^{\alpha}u) + \phi(D_{yy}^{\alpha}u) + 2\phi(D_{xy}^{\alpha}u) \Big] \Big\} \quad (15)$$

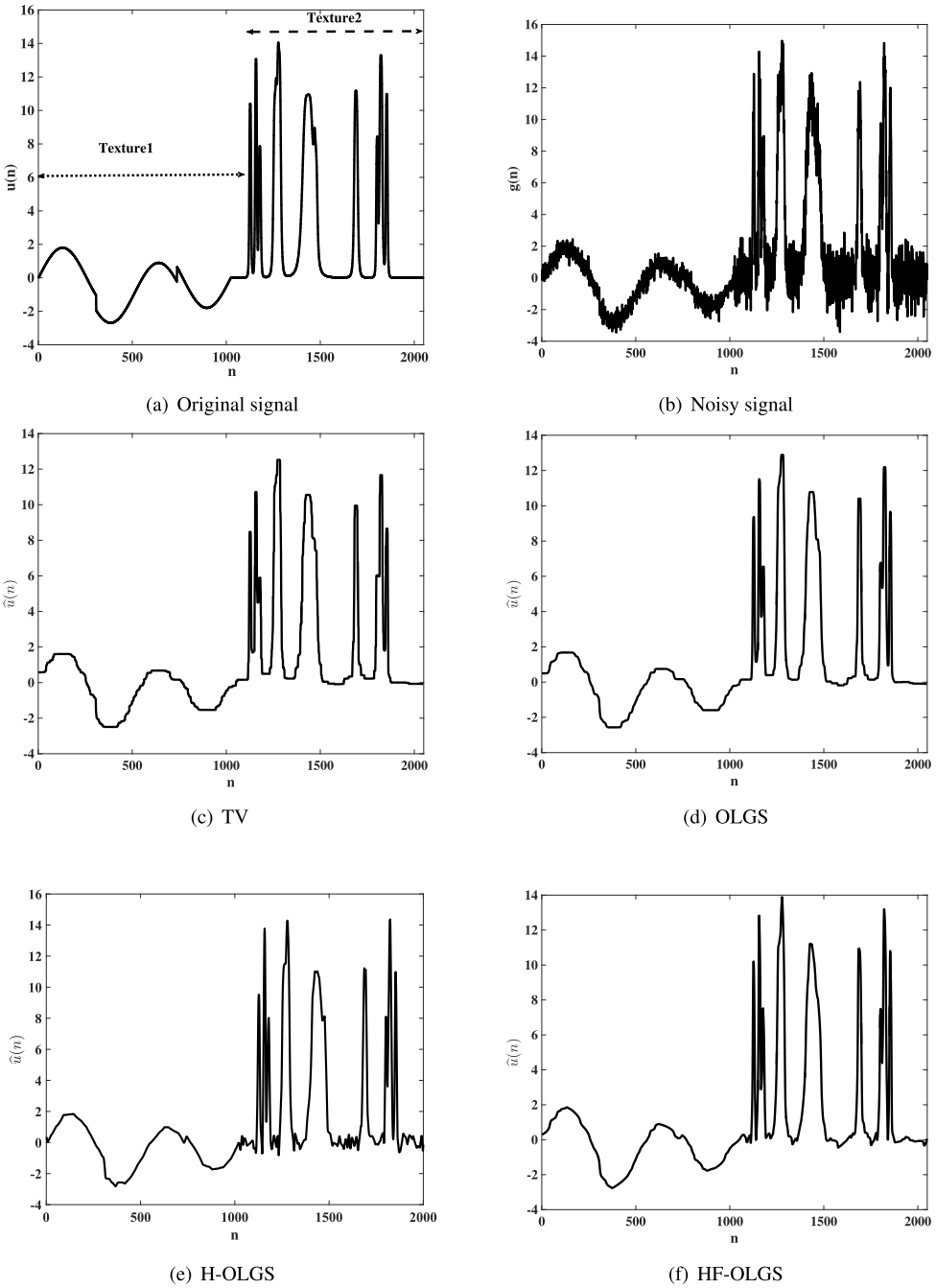

(a) Original signal (b) Noisy signal

(c) TV (d) OLGS

(e) H-OLGS (f) HF-OLGS

FIGURE 2. Restoration of test signal (*Texture*1 + *Texture*2) using TV, OLGS, H-OLGS and HF-OLGS regularizers. (a) Original signal. (b) Noisy signal. (c) TV. (d) OLGS. (e) H-OLGS. (f) HF-OLGS.

where the data fidelity term is given as

$$E(u,g) = \begin{cases} ||Hu - g||_2^2, & \text{Gaussian.} \\ Hu - g\log(Hu), & \text{Poisson.} \end{cases} \tag{16}$$

This framework is formulated to evaluate the restoration quality of the images degraded due to Gaussian and Poisson noise using the proposed regularizer. The alternating direction method of multipliers (ADMM) method having the capability of rapidly obtaining the stable convergence is used in the proposed optimization framework. With the introduction of new auxiliary variables $v_1 = [v_{1:x} \;\; v_{1:y}]^T$ and $v_2 = [v_{2:xx} \;\; v_{2:yy} \;\; v_{2:xy}]^T$, the minimization problem stated in (15) can be formulated as an equivalent constrained minimization problem as

$$\min_{u,v_1,v_2} \Big\{ Z = E(u,g) + \beta_1 \big[\phi(v_{1:x}) + \phi(v_{1:y}) \big] + \beta_2 \big[\phi(v_{2:xx}) + \phi(v_{2:yy}) + 2\phi(v_{2:xy}) \big] \Big\} \tag{17}$$

such that $v_{1:x} = D_x^\alpha u, v_{1:y} = D_y^\alpha u, v_{2:xx} = D_{xx}^\alpha u, v_{2:yy} = D_{yy}^\alpha u$ and $v_{2:xy} = D_{xy}^\alpha u$. The augmented Lagrangian function corresponding to the minimization problem (17) can be written

as

$$
\begin{aligned}
&L_{\gamma_1,\gamma_2}(u, v_1, v_2)\\
&=\Bigg\{E(u,g)+\beta_1\left[\phi(v_{1:x})+\phi(v_{1:y})\right]\\
&\quad+\beta_2\left[\phi(v_{2:xx})+\phi(v_{2:yy})+2\phi(v_{2:xy})\right]\\
&\quad+\frac{\gamma_1}{2}\left[\left\|D_x^\alpha u-v_{1:x}+\frac{p_{1:x}}{\gamma_1}\right\|_2^2+\left\|D_y^\alpha u-v_{1:y}+\frac{p_{1:y}}{\gamma_1}\right\|_2^2\right]\\
&\quad+\frac{\gamma_2}{2}\left[\left\|D_{xx}^\alpha u-v_{2:xx}+\frac{p_{2:xx}}{\gamma_2}\right\|_2^2+\left\|D_{yy}^\alpha u-v_{2:yy}+\frac{p_{2:yy}}{\gamma_2}\right\|_2^2\right.\\
&\quad\left.+2\left\|D_{xy}^\alpha u-v_{2:xy}+\frac{p_{2:xy}}{\gamma_2}\right\|_2^2\right]\Bigg\} \qquad (18)
\end{aligned}
$$

where $\beta_1, \beta_2 > 0$ and $p_1 = [p_{1:x}\ \ p_{1:y}]^T$ and $p_2 = [p_{2:xx}\ p_{2:yy}\ p_{2:xy}]^T$ are the Lagrangian multipliers.

According to ADMM (Sec. II-C), we need to solve the subproblems involved with variables u, v_1 and v_2 present in the Lagrangian defined in (18) one by one. We now investigate the first sub-problem involving the variable u. This sub-problem corresponds to the following optimization problem:

$$
\begin{aligned}
\min_u\Bigg\{E(u,g)&+\frac{\gamma_1}{2}\left[\left\|D_x^\alpha u-v_{1:x}+\frac{p_{1:x}}{\gamma_1}\right\|_2^2\right.\\
&\left.+\left\|D_y^\alpha u-v_{1:y}+\frac{p_{1:y}}{\gamma_1}\right\|_2^2\right]\\
&+\frac{\gamma_2}{2}\left[\left\|D_{xx}^\alpha u-v_{2:xx}+\frac{p_{2:xx}}{\gamma_2}\right\|_2^2\right.\\
&\left.+\left\|D_{yy}^\alpha u-v_{2:yy}+\frac{p_{2:yy}}{\gamma_2}\right\|_2^2\right.\\
&\left.+2\left\|D_{xy}^\alpha u-v_{2:xy}+\frac{p_{2:xy}}{\gamma_2}\right\|_2^2\right]\Bigg\} \qquad (19)
\end{aligned}
$$

With the image degraded due to Gaussian noise, the data fidelity term in (19) is given as $E(u,g) = ||Hu-g||_2^2$, resulting in the following optimization problem:

$$
\begin{aligned}
\min_u\Bigg\{&\|Hu-g\|_2^2+\frac{\gamma_1}{2}\left[\left\|D_x^\alpha u-v_{1:x}+\frac{p_{1:x}}{\gamma_1}\right\|_2^2\right.\\
&\left.+\left\|D_y^\alpha u-v_{1:y}+\frac{p_{1:y}}{\gamma_1}\right\|_2^2\right]+\frac{\gamma_2}{2}\left[\left\|D_{xx}^\alpha u-v_{2:xx}+\frac{p_{2:xx}}{\gamma_2}\right\|_2^2\right.\\
&\left.+\left\|D_{yy}^\alpha u-v_{2:yy}+\frac{p_{2:yy}}{\gamma_2}\right\|_2^2+2\left\|D_{xy}^\alpha u-v_{2:xy}+\frac{p_{2:xy}}{\gamma_2}\right\|_2^2\right]\Bigg\} \qquad (20)
\end{aligned}
$$

The minimization of sub-problem stated in (20) with respect to u is the standard least square problem which is equivalent to the (21), as shown at the bottom of this page.

Here, i is the iteration variable and the fast Fourier transform and its inverse is denoted by F and F^{-1} respectively. It should be noted that the operators in (21) i.e. H, D_x^α, D_y^α, $D_{xx,}^\alpha$, D_{yy}^α and D_{xy}^α are highly structured matrices. However, their exact structure depends on the boundary conditions imposed on the image under consideration. In this work, we have adopted the periodic boundary conditions that enable these operators to have block circulant with circulant blocks (BCCB) structure. This helps in computing these BCCB matrices using fast Fourier transforms.

Next, if the image is degraded due to Poisson noise, the data fidelity term in (19) is given as $E(u,g) = (Hu - g\log(Hu))$ resulting in the following optimization problem:

$$
\begin{aligned}
\min_u\Bigg\{&(Hu-g\log(Hu))+\frac{\gamma_1}{2}\left[\left\|D_x^\alpha u-v_{1:x}+\frac{p_{1:x}}{\gamma_1}\right\|_2^2\right.\\
&\left.+\left\|D_y^\alpha u-v_{1:y}+\frac{p_{1:y}}{\gamma_1}\right\|_2^2\right]+\frac{\gamma_2}{2}\left[\left\|D_{xx}^\alpha u-v_{2:xx}+\frac{p_{2:xx}}{\gamma_2}\right\|_2^2\right.\\
&\left.+\left\|D_{yy}^\alpha u-v_{2:yy}+\frac{p_{2:yy}}{\gamma_2}\right\|_2^2+2\left\|D_{xy}^\alpha u-v_{2:xy}+\frac{p_{2:xy}}{\gamma_2}\right\|_2^2\right]\Bigg\} \qquad (22)
\end{aligned}
$$

With the introduction of the auxiliary variable $w = Hu$, the optimization problem stated in (22) can be reformulated as

$$
\begin{aligned}
\min_{u,w}\Bigg\{&(w-f\log w)+\sigma\|Hu-w+b_1\|_2^2\\
&+\frac{\gamma_1}{2}\left[\left\|D_x^\alpha u-v_{1:x}+\frac{p_{1:x}}{\gamma_1}\right\|_2^2+\left\|D_y^\alpha u-v_{1:y}+\frac{p_{1:y}}{\gamma_1}\right\|_2^2\right]\\
&+\frac{\gamma_2}{2}\left[\left\|D_{xx}^\alpha u-v_{2:xx}+\frac{p_{2:xx}}{\gamma_2}\right\|_2^2+\left\|D_{yy}^\alpha u-v_{2:yy}+\frac{p_{2:yy}}{\gamma_2}\right\|_2^2\right.\\
&\left.+2\left\|D_{xy}^\alpha u-v_{2:xy}+\frac{p_{2:xy}}{\gamma_2}\right\|_2^2\right]\Bigg\} \qquad (23)
\end{aligned}
$$

The minimization of (23) with respect to u is given as

$$
\begin{aligned}
\min_u\Bigg\{&\sigma\|Hu-w+b_1\|_2^2+\frac{\gamma_1}{2}\left[\left\|D_x^\alpha u-v_{1:x}+\frac{p_{1:x}}{\gamma_1}\right\|_2^2\right.\\
&\left.+\left\|D_y^\alpha u-v_{1:y}+\frac{p_{1:y}}{\gamma_1}\right\|_2^2\right]+\frac{\gamma_2}{2}\left[\left\|D_{xx}^\alpha u-v_{2:xx}+\frac{p_{2:xx}}{\gamma_2}\right\|_2^2\right.\\
&\left.+\left\|D_{yy}^\alpha u-v_{2:yy}+\frac{p_{2:yy}}{\gamma_2}\right\|_2^2+2\left\|D_{xy}^\alpha u-v_{2:xy}+\frac{p_{2:xy}}{\gamma_2}\right\|_2^2\right]\Bigg\} \qquad (24)
\end{aligned}
$$

The solution of (24) is similar to that of (20) i.e. the standard least square problem whose solution is obtained using the (25), as shown at the bottom of the next page.

$$
u^{i+1}=F^{-1}\left\{F^{-1}\left\{\frac{H^*g+\gamma_1\left[\left(D_x^\alpha\right)^*\left(v_{1:x}^i-\frac{p_{1:x}^i}{\gamma_1}\right)+\left(D_y^\alpha\right)^*\left(v_{1:y}^i-\frac{p_{1:y}^i}{\gamma_1}\right)\right]+\gamma_1\left[\left(D_{xx}^\alpha\right)^*\left(v_{2:xx}^i-\frac{p_{2:xx}^i}{\gamma_2}\right)+\left(D_{yy}^\alpha\right)^*\left(v_{2:yy}^i-\frac{p_{2:yy}^i}{\gamma_2}\right)+2\left(D_{xy}^\alpha\right)^*\left(v_{2:xy}^i-\frac{p_{2:xy}^i}{\gamma_2}\right)\right]}{H^*H+\gamma_1\left[\left(D_x^\alpha\right)^*\left(D_x^\alpha\right)+\left(D_y^\alpha\right)^*\left(D_y^\alpha\right)\right]+\left[\gamma_2\left(D_{xx}^\alpha\right)^*\left(D_{xx}^\alpha\right)+\left(D_{yy}^\alpha\right)^*\left(D_{yy}^\alpha\right)+2\left(D_{xy}^\alpha\right)^*\left(D_{xy}^\alpha\right)\right]}\right\}\right\} \qquad (21)
$$

The minimization of (23) with respect to the auxiliary variable w is given as

$$\min_{w} \left\{ (w - f \log w) + \frac{\sigma}{2} \|Hu - w + b_1\|_2 \right\} \tag{26}$$

The solution to (26) is obtained as

$$w^{i+1} = \frac{1}{2}\left[\left(Hu^{i+1} + b_1^i - \frac{1}{\sigma}\right) + \sqrt{\left(Hu^{i+1} + b_1^i - \frac{1}{\sigma}\right)^2 + \frac{4g}{\sigma}}\right] \tag{27}$$

The variable b_1 is updated as

$$b_1^{i+1} = b_1^i + (Hu^{i+1} - w^{i+1}) \tag{28}$$

The restored image u degraded due to Gaussian or Poisson noise is obtained via the solutions stated in (21) and (25) corresponding to the optimization problems (20) and (24), respectively. Once the variable u is optimized, the components of the auxiliary variable v_1 which is common to both types of noise is minimized using (18) as the following sub-problems

$$v_{1:x}^{i+1} = \underset{v_{1:x}}{\operatorname{argmin}} \left[\beta_1 \phi(v_{1:x}) + \frac{\gamma_1}{2} \left\| D_x^\alpha u^{i+1} - v_{1:x} + \frac{p_{1:x}^i}{\gamma_1} \right\|_2^2 \right] \tag{29}$$

$$v_{1:y}^{i+1} = \underset{v_{1:x}}{\operatorname{argmin}} \left[\beta_1 \phi(v_{1:y}) + \frac{\gamma_1}{2} \left\| D_y^\alpha u^{i+1} - v_{1:y} + \frac{p_{1:y}^i}{\gamma_1} \right\|_2^2 \right] \tag{30}$$

Similarly the components of the vector v_2 are minimized as

$$v_{2:xx}^{i+1} = \underset{v_{2:xx}}{\operatorname{argmin}} \left[\beta_2 \phi(v_{2:xx}) + \frac{\gamma_2}{2} \left\| D_{xx}^\alpha u^{i+1} - v_{2:xx} + \frac{p_{2:xx}^i}{\gamma_2} \right\|_2^2 \right] \tag{31}$$

$$v_{2:yy}^{i+1} = \underset{v_{2:yy}}{\operatorname{argmin}} \left[\beta_2 \phi(v_{2:yy}) + \frac{\gamma_2}{2} \left\| D_{yy}^\alpha u^{i+1} - v_{2:yy} + \frac{p_{2:yy}^i}{\gamma_2} \right\|_2^2 \right] \tag{32}$$

$$v_{2:xy}^{i+1} = \underset{v_{2:xy}}{\operatorname{argmin}} \left[\beta_2 \phi(v_{2:xy}) + \frac{\gamma_2}{2} \left\| D_{xy}^\alpha u^{i+1} - v_{2:xy} + \frac{p_{2:xy}^i}{\gamma_2} \right\|_2^2 \right] \tag{33}$$

The solution to the above minimization problem stated in (29)-(33) can be solved effectively using the method of majorization and minimization for which the details can be found in [40], [50], and [51]. Finally, the Lagrangian multipliers. p_1 and p_2 are updated as

$$p_{1:x}^{i+1} = p_{1:x}^i + \gamma_1 (D_x^\alpha u^{i+1} - v_{1:x}^{i+1}) \tag{34}$$

$$p_{1:y}^{i+1} = p_{1:y}^i + \gamma_1 (D_y^\alpha u^{i+1} - v_{1:y}^{i+1}) \tag{35}$$

$$p_{2:xx}^{i+1} = p_{2:xx}^i + \gamma_2 (D_{xx}^\alpha u^{i+1} - v_{1:xx}^{i+1}) \tag{36}$$

$$p_{2:yy}^{i+1} = p_{2:yy}^i + \gamma_2 (D_{yy}^\alpha u^{i+1} - v_{1:yy}^{i+1}) \tag{37}$$

$$p_{2:xy}^{i+1} = p_{2:xy}^i + \gamma_2 (D_{xy}^\alpha u^{i+1} - v_{2:xy}^{i+1}) \tag{38}$$

Algorithm 1 Solving the Optimization Framework (15) for **Gaussian** Noise

Initialization:

Starting point: $(v_1,\ v_2 = g)$; $(p_1,\ p_2 = 0)$; $(\beta_1,\ \beta_2,\ \gamma_1,\ \gamma_2 > 0)$, K

Iterations:

For i = 1 to MaxIter

1) Compute u^{i+1} according to (21)
2) Compute v_1^{i+1} according to (29)-(30)
3) Compute v_2^{i+1} according to (31)-(33)
4) Compute p_1^{i+1} according to (34)-(35)
5) Compute p_2^{i+1} according to (36)-(38)
6) *until a stopping criterion is satisfied stated in* (39)

Algorithm 2 Solving the Optimization Framework (15) for **Poisson** Noise

Initialization:

Starting point: $(v_1,\ v_2,\ w = g)$; $(p_1,\ p_2,\ b_1 = 0)$; $(\beta_1,\ \beta_2,\ \gamma_1,\ \gamma_2,\ \sigma > 0)$, K

Iterations:

For i = 1 to MaxIter

1) Compute u^{i+1} according to (25)
2) Compute v_1^{i+1} according to (29)-(30)
3) Compute v_2^{i+1} according to (31)-(33)
4) Compute w^{i+1} according to (27)
5) Compute b_1^{i+1} according to (28)
6) Compute p_1^{i+1} according to (34)-(35)
7) Compute p_2^{i+1} according to (36)-(38)
8) *until a stopping criterion is satisfied stated in* (39)

Based on the above discussion, the proposed optimization framework for Gaussian and Poisson noise is presented as **Algorithms** 1 and 2, respectively.

$$u^{i+1} = F^{-1}\left\{ F\left\{ \frac{\sigma H^*(w^i - b_1^i) + \gamma_1 \left[\left(D_x^\alpha\right)^* \left(v_{1:x}^i - \frac{p_{1:x}^i}{\gamma_1}\right) + \left(D_y^\alpha\right)^* \left(v_{1:y}^i - \frac{p_{1:y}^i}{\gamma_1}\right) \right] + \gamma_1 \left[\left(D_{xx}^\alpha\right)^* \left(v_{2:xx}^i - \frac{p_{2:xx}^i}{\gamma_2}\right) + \left(D_{yy}^\alpha\right)^* \left(v_{2:yy}^i - \frac{p_{2:yy}^i}{\gamma_2}\right) + 2\left(D_{xy}^\alpha\right)^* \left(v_{2:xy}^i - \frac{p_{2:xy}^i}{\gamma_2}\right) \right]}{\sigma H^T H + \gamma_1 \left[\left(D_x^\alpha\right)^* \left(D_x^\alpha\right) + \left(D_y^\alpha\right)^* \left(D_y^\alpha\right) \right] + \gamma_2 \left[\left(D_{xx}^\alpha\right)^* \left(D_{xx}^\alpha\right) + \left(D_{yy}^\alpha\right)^* \left(D_{yy}^\alpha\right) + 2\left(D_{xy}^\alpha\right)^* \left(D_{xy}^\alpha\right) \right]} \right\} \right\} \tag{25}$$

A. CONVERGENCE ANALYSIS

The convexity of the energy function defined in (15) is convex for both the Gaussian and Poisson cases. Please see Appendix A for proof. In view of this convexity, the convergence of **algorithms** 1 and 2 is guaranteed via the ADMM theory [41]. The system governing variables involved in the algorithms, namely, u, v_1, v_2 and w is decoupled into their own sub-problems and these sub-problems have closed form solutions. For instance, the sub-problem involving variable u is solved using conjugate gradient method [49], which is convergent with structured matrices $(D_x^\alpha)^* D_x^\alpha$, $(D_y^\alpha)^* D_y^\alpha$, $(D_{xx}^\alpha)^* D_{xx}^\alpha$, $(D_{yy}^\alpha)^* D_{yy}^\alpha$ and $(D_{xy}^\alpha)^* D_{xy}^\alpha$ being positive definite and invertible. Here, we assume periodic boundary conditions that enable these matrices to be block circulant with circulant blocks (BCCB) structure. The variables v_1 and v_2 are solved using majorization-minimization algorithm which is proved to be convergent in [40]. The sub-problem involving variable w is a differential function which can be easily minimized. The stopping criterion used in the two algorithms is

$$RelErr = \frac{\left\|u^{i+1} - u^i\right\|_2}{\left\|u^{i+1}\right\|_2} < 10^{-3} \quad or \quad i = MaxIter \tag{39}$$

we set MaxIter = 100 in this paper. Here, u^i is the computationally accepted approximation of the original image when the relative difference between the consecutive approximations satisfies the stopping criterion. Fig. 3 shows the evolution of *RelErr* as a function of the number of iterations for the two algorithms. It can be observed from this figure that the error decreases monotonically with iterations, confirming the convergence behaviour of the two algorithms.

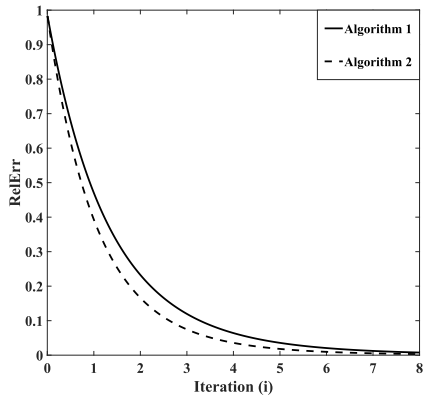

FIGURE 3. Evolution of RelErr as a functions of the number of iterations for the two algorithms.

V. EXPERIMENTAL RESULTS AND ANALYSIS

The aim of this section is to demonstrate the performance of the proposed HF-OLGS based image denoising framework. For this purpose, simulations are carried on using six different gray-scale images of varying texture content shown in Fig 4. To prove the effectiveness of the proposed algorithm on real databases, we have selected LIVE [50] database for evaluation. To quantify the quality of the restored image, widely used image metrics peak-signal-to-noise ration (PSNR) and Structural SIMilarity (SSIM) [51] index are adopted. These metrics are evaluated as follows: PSNR is defined as

$$PSNR = 10\log_{10}\left(\frac{255^2 MN}{\sum_{i=0}^{M-1}\sum_{i=0}^{N-1}(u(i,j) - \widehat{u}(i,j))^2}\right) \tag{40}$$

where u is the original image and $\widehat{u}$ is the denoised image. Higher the PSNR value, better is the image quality. The Structural SIMilarity (SSIM) index is a method for measuring the similarity between two images. SSIM index can be viewed as a quality measure of one of the images being compared, provided the other image is regarded as of perfect quality. SSIM for the two images x and y is defined as

$$SSIM(x,y) = \frac{(2\mu_x\mu_y + c_1)(2\sigma_{xy} + c_2)}{(\mu_x^2 + \mu_y^2 + c_1)(\sigma_x^2 + \sigma_y^2 + c_2)} \tag{41}$$

where μ_x and μ_y are the averages of x and y respectively, σ_x^2 and σ_y^2 are the variances of x and y, σ_{xy}^2 is the covariance of x and y while c_1, c_2 are the two variables to stabilize the division with weak denominator. SSIM is less than or equal to 1 and it is maximal when the two images are coincide. All the experiments are carried out on Mac OS 10.12 and MATLAB v15 running on a desktop equipped with an Intel Core i7 CPU 2.2 GHz and 16 GB of RAM.

A. STUDY ON GROUP SIZE (K) AND FRACTIONAL ORDER (α)

With the use of fractional order derivatives in the proposed regularizer presented in (13), it has been observed that the performance of the regularizer depends on the optimal selection of group size (K) and fractional order (α). Hence, it becomes important to understand the role played by these parameters in order to achieve an effective state of the art denoising results. Furthermore, as discussed in Sec.III regarding the performance of the proposed regularizer in case of one-dimensional signal, a similar analysis needs to be carried out for two dimensional signals in order to justify the applicability of the proposed regularizer. In order to do this, six standard test images of *baboon*, *barbara*, *cameraman*, *parrot*, *lena* and *house* are selected for evaluation as shown in Figs.4(a)-(f). The first 3 test images, namely, (a) Baboon, (b) Barbara and (c) Cameraman are of size 512 × 512, while the last three images; (d) Parrot, (e) Lena and (f) House are of size 256 × 256. These images are selected based on their varying texture content as shown in Figs.4(g)-(l). Here, the black region corresponds to plain patches, grey region corresponds to edge patches and white region corresponds to texture patches. The reason for arranging them in terms of the texture content is to show the effectiveness of the proposed regularizer in restoring the texture content as was done in the case of one-dimensional signals shown in Figs. 1-2. There are several methods proposed in the literature for carrying out image decomposition into plain (P), edge (E) and texture (T)

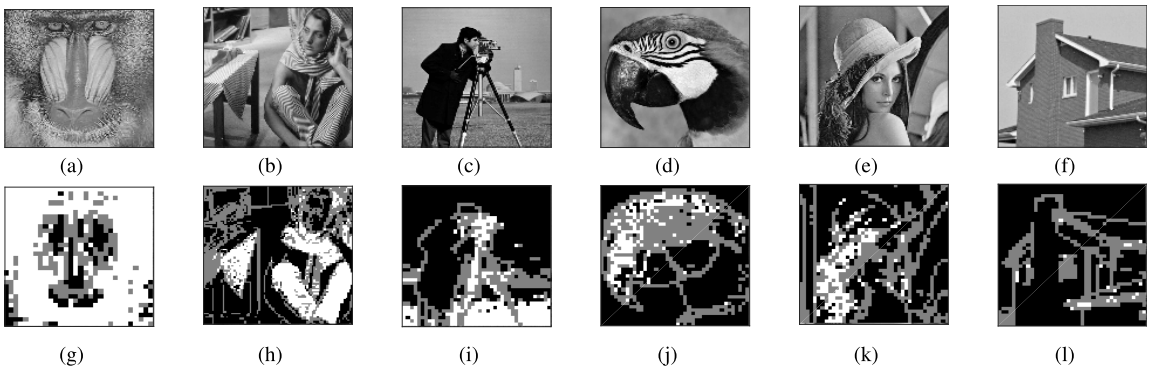

FIGURE 4. (a)-(f) Standard test images of *baboon*, *barbara*, *cameraman*, *parrot*, *lena* and *house*. (g)-(l) Plain, Edge and Texture classification map of test images. Here, black corresponds to plain patch, grey corresponds to edge patch and white corresponds to texture patch. Images are arranged from left to right in descending order of the texture contribution.

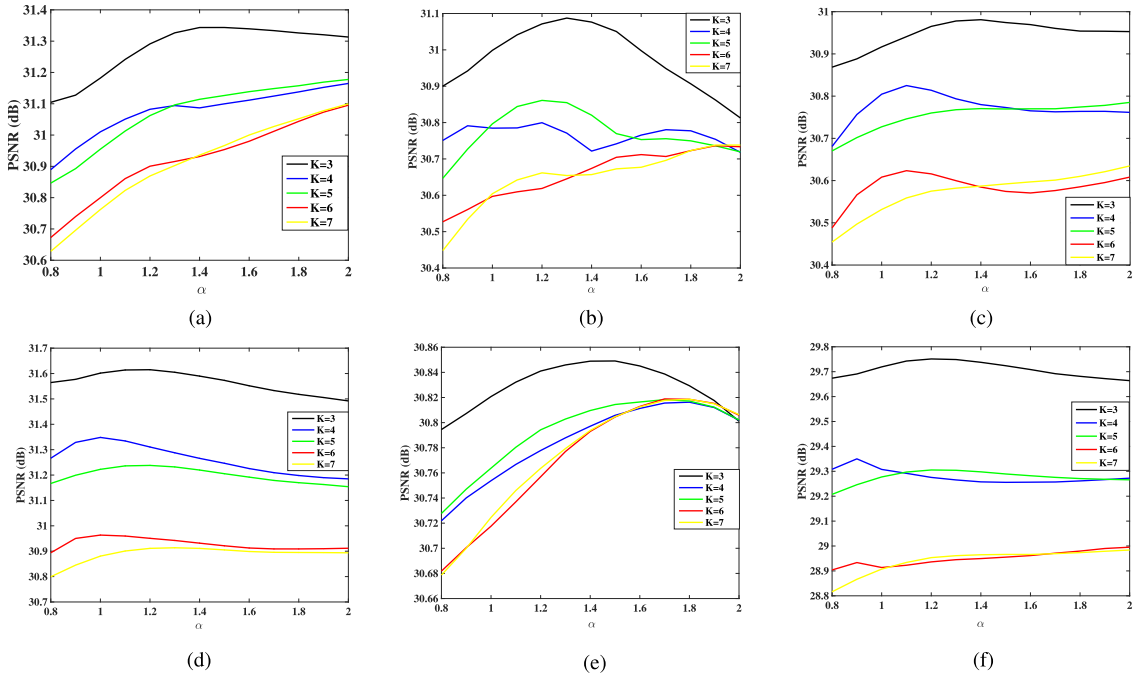

FIGURE 5. Effect of group size (K) and fractional order (α) on PSNR of the restored images degraded by (a)-(c) Gaussian noise (d)-(f) Poisson noise. (a) *baboon*. (b) *barbara*. (c) *cameraman*. (d) *parrot*. (e) *lena*. (f) *house*.

blocks [52]–[56]. In this paper, we have adopted the method proposed by Zhang *et al.* [53] that utilizes discrete cosine transform (DCT) coefficients for carrying out the image decomposition task.

The values of (K, α) are selected based on experimental work as follows. Figs. 5 and 6 show the PSNR and SSIM variations as a function of parameters K and α for the test images shown in Figs. 4(a)-(f). The first three images are subjected to Gaussian noise of standard deviation 20, while the last three are subjected to Poisson noise. It can be observed that the maximum value of PSNR as well as that of SSIM is achieved for $K = 3$ and $\alpha = (1.2, 1.3, 1.4)$. This shows that the selection of the parameter K is independent of the texture content in an image. However, the value of the fractional coefficient α depends on the texture content. Further, the selected value of α confirms the findings in [20] regarding the optimal values of α for effective texture restoration. Other parameters used in the algorithms are taken as follows: **Algorithm 1**: $\beta_1 = 1e-6$, $\beta_2 = 0.8$, $\gamma_1 = 0.33e-6$ and $\gamma_2 = 0.26$. For **Algorithm 2**: $\beta_1 = 1e-3$, $\beta_2 = 0.1$, $\gamma_1 = 0.25e-3$, $\gamma_2 = 0.04$ and $\sigma = 1e4$.

B. TEXTURE ANALYSIS

The discussion carried out in Figs. 5 and 6 is a kind of quantitative evaluation of the proposed algorithm. In order to see the impact of the parameters (K, α) on the quality of the image restored, visual comparisons are performed using various values of (K, α) on the images of *parrot* and *barbara*

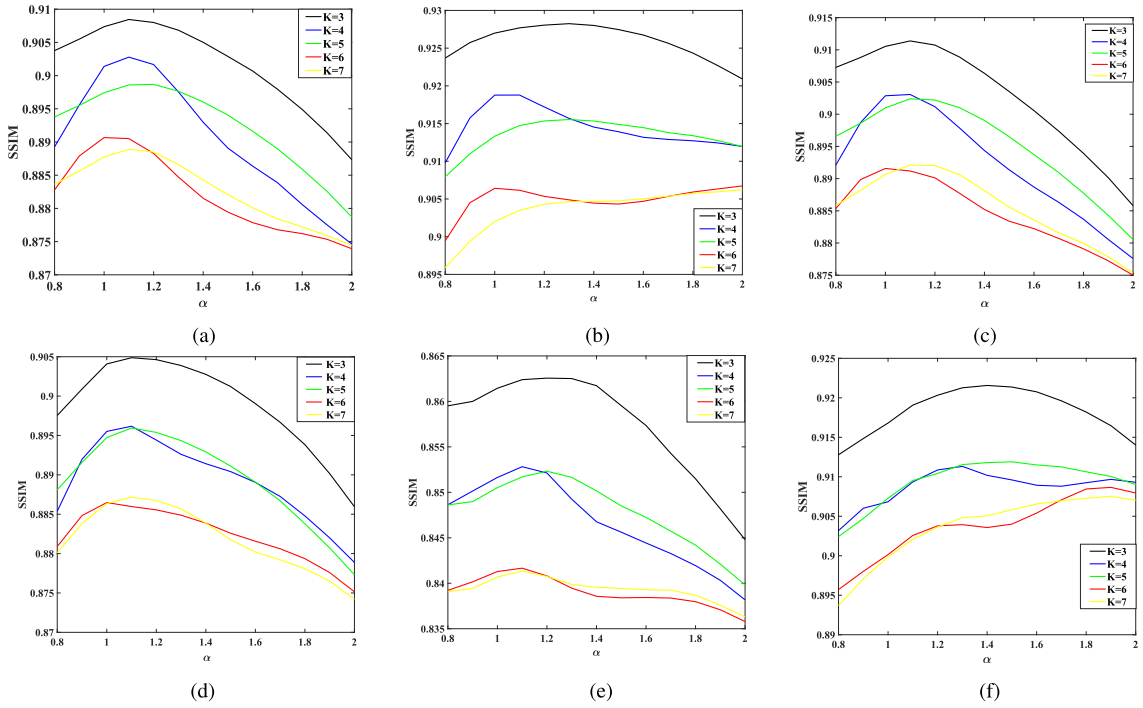

FIGURE 6. Effect of group size (K) and fractional order (α) on SSIM of the restored images degraded by (a)-(c) Gaussian noise (d)-(f) Poisson noise. (a) *baboon*. (b) *barbara*. (c) *cameraman*. (d) *parrot*. (e) *lena*. (f) *house*.

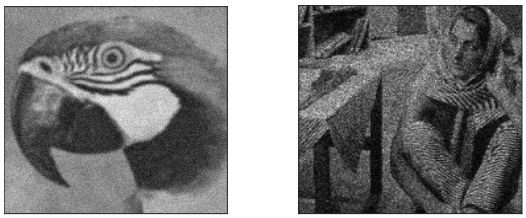

FIGURE 7. Noisy images of (a) *parrot* (b) *barbara* subjected to Gaussian and Poisson noise respectively.

degraded due to Gaussian of standard deviation 20 and Poisson noise, respectively. Fig. 7 shows the degraded images of *parrot* and *barbara*, whereas Figs.8-9 show their respective restored versions. The results in Fig 8 show that for ($K = 3$, $\alpha = 1.2$), the proposed fractional model preserve the fine textures in an image. However, for other values of (K, α), the fine textures of the restored images are degraded due to the presence of small Gaussian noise appearing in the texture images as shown in Figs. 8(e)-(g). Similarly for the case of restored versions of *barbara* image shown in Fig 7, it can be observed that effective texture restoration is obtained for ($K = 3, \alpha = 1.4$) while for other cases some Poisson noise penetrates into the texture component of the restored images as shown in Figs. 9(e)-(g).

C. COMPARATIVE ANALYSIS

The proposed denoising framework is developed for restoring the images degraded due to Gaussian and Poisson noise. Hence, it becomes essential to compare the quality of the restored image with the other state-of-the-art algorithms. For this purpose, in the case of Gaussian noise we have selected the methods proposed by Cuesta *et al.* [38], fractional-order total variation using proximity algorithm (FTV-PA) [57], R-NL [58], Adaptive Regularization with the Structure Tensor [59]., the full fractional anisotropic diffusion (FFAD) [60] and overlapping group sparsity (OLGS) [40] for comparative analysis. For the case of Poisson noise, comparison is performed with the methods such as fourth-order partial differential equation filter (FOPDEF) [12], TV-Poi [61], OGS-ADM [62], Framelet based (BPID-FR) [63], spatially adaptive (RLSATV) [64] and sparse based (TV-L0) [65]. The work of TV-Poi and OGS-ADM is based on the TV and overlapping group sparsity based prior for Poisson noise image deblurring. The FOPDEF algorithm uses higher order partial differential equations for removing Poisson noise with staircase reduction.

In this work, we consider blurring operator H to be Gauss ($\mathbf{G}$) blur kernel [66]. It has two parameters to its definition, namely, bandwidth (s) and standard deviation (η). In our set of experiments, we set these parameters as $s = 11$ and $\eta = 2.3$. In order to simulate noisy operations after blurring the original images with $\mathbf{G}$, two sets of experiments are created. In the first set, we add Poisson noise to the image using *poissrnd* function from the MATLAB toolbox to generate blurred and noisy images shown in Figs 10(a) and 11(a). The magnitude of the noise directly depends on the absolute image intensities. In the second set, an additive white Gaussian noise (AWGN) with standard deviation of 20 and

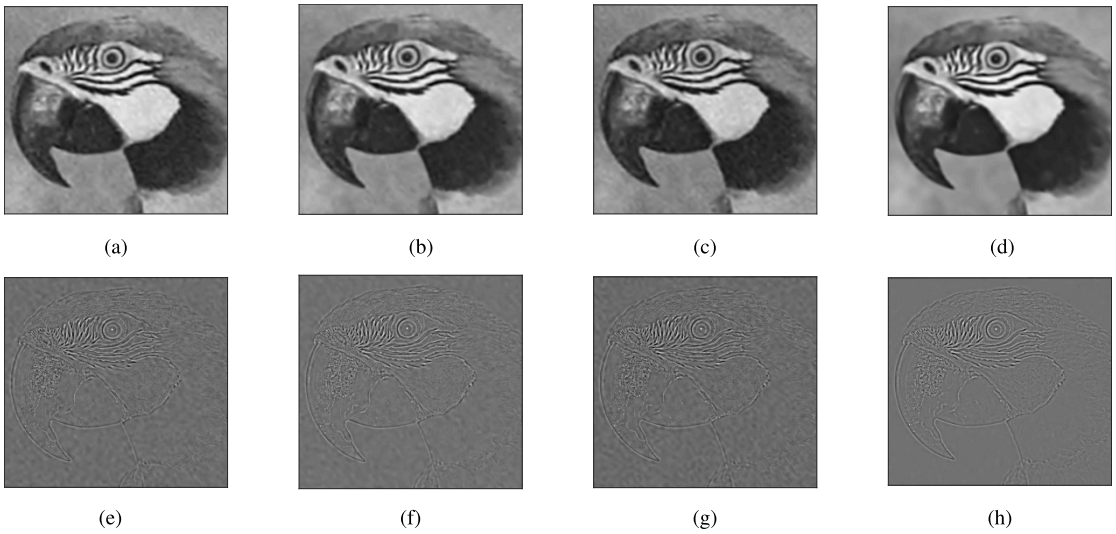

FIGURE 8. (a)-(d) Visual comparison of the restored image of *parrot* shown in Fig. 7(a) for various values of the parameters K and α. (e)-(h) Corresponding texture details. (a) $K = 3$, $\alpha = 0.8$. (b) $K = 3$, $\alpha = 1.0$. (c) $K = 3$, $\alpha = 1.4$. (d) $K = 3$, $\alpha = 1.2$. (e) $K = 3$, $\alpha = 0.8$. (f) $K = 3$, $\alpha = 1.0$. (g) $K = 3$, $\alpha = 1.4$. (h) $K = 3$, $\alpha = 1.2$.

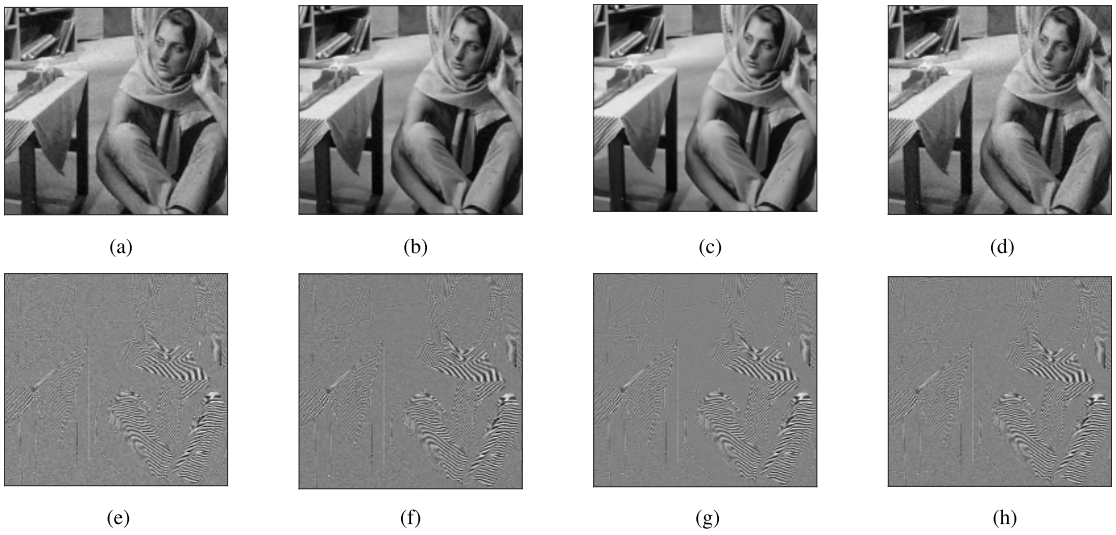

FIGURE 9. (a)-(d) Visual comparison of the restored image of *barbara* shown in Fig. 7(b) for various values of the parameters K and α. (e)-(h) Corresponding texture details. (a) $K = 3$, $\alpha = 0.8$. (b) $K = 3$, $\alpha = 1.0$. (c) $K = 3$, $\alpha = 1.3$. (d) $K = 3$, $\alpha = 1.4$. (e) $K = 3$, $\alpha = 0.8$. (f) $K = 3$, $\alpha = 1.0$. (g) $K = 3$, $\alpha = 1.3$. (h) $K = 3$, $\alpha = 1.4$.

30 is added to the test images blurred using $\mathbf{G}$ as shown in Figs 12(a) and 13(a) respectively.

For the first set of experiments dealing with Poisson noise, we have taken images of *cameraman* and *house* for our study. Both of these images are blurred using Gauss blur and additionally contaminated using Poisson noise as shown in Figs 10(a) and 11(a). For the case of *cameraman* image, Figs. 10(b)-(h) show the restoration results using seven different methods. It is not difficult to observe that the proposed method (HF-OLGS) is better than the other methods in restoring the textures of an image. The face and nose of the *cameraman* and the texture of the building in the background are restored well using TV-L0 and our method when compared to other methods. Furthermore, undesirable staircase effects are minimized using the proposed method, thus providing better image visual quality. Similarly, for the *house* image, Figs. 11(b)-(h) shows the restored quality obtained using different methods. It can be observed that the roof texture and the edges around the windows as well as around the boundary of the house are preserved to a greater extent when compared to that in the other methods.

For the second set of experiments dealing with Gaussian noise, images of *lena* and *barbara* are taken for testing the effectiveness of the proposed algorithm. Both of these images are blurred using Gauss blur of size $s = 11$ and additionally degraded using additive white Gaussian

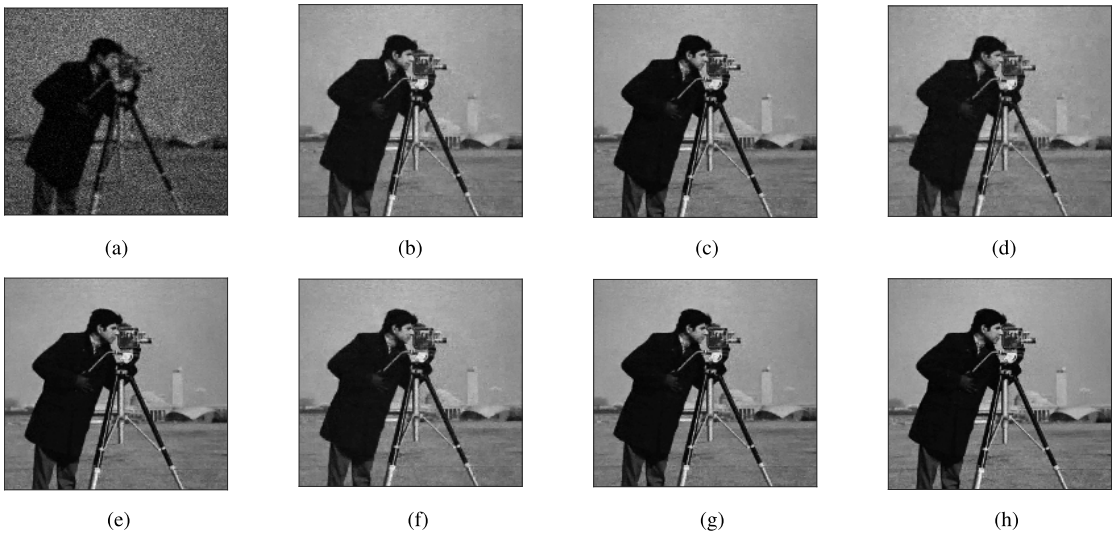

FIGURE 10. Denoising results for the image *cameraman* under the Gauss blur (*G*) and Poisson noise (a) Noisy image (b) **FOPDEF**, PSNR (SSIM) = 27.82(0.751); (c) **BPID-FR**, PSNR (SSIM) = 28.04(0.781); (d) **OGS-ADM**, PSNR (SSIM) = 28.18(0.802); (e) **RLSATV**, PSNR (SSIM) = 28.78(0.821); (f) **TV-Poi**, PSNR(SSIM) = 29.06(0.841); (g) **TV-L0**, PSNR(SSIM) = 29.52(0.883) (h) **HF-OLGS**, PSNR(SSIM) = 30.37(0.912). (a) Noisy image.

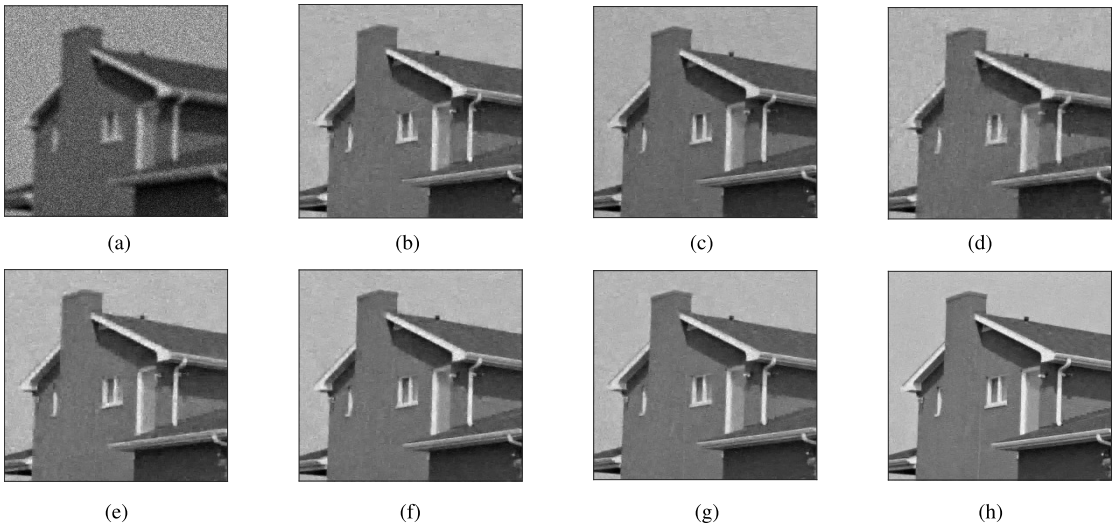

FIGURE 11. Denoising results for the image *house* under the Gauss blur (*G*) and Poisson noise (a) Noisy image (b) **FOPDEF**, PSNR (SSIM) = 26.12(0.724); (c) **BPID-FR**, PSNR (SSIM) = 27.04(0.732); (d) **OGS-ADM**, PSNR (SSIM) = 27.78(0.747); (e) **RLSATV**, PSNR (SSIM) = 28.18(0.809); (f) **TV-Poi**, PSNR(SSIM) = 28.87(0.863); (g) **TV-L0**, PSNR(SSIM) = 29.12(0.873) (h) **HF-OLGS**, PSNR(SSIM) = 30.12(0.903). (a) Noisy image.

noise with standard deviation of 20 and 30, respectively, as shown in Figs. 12(a) and 13(a). Their corresponding restored versions using seven different methods are shown in Figs. 12(b)-(h) and Figs. 13(b)-(h), respectively. It can be observed clearly that the proposed method restores the texture components present in the hat and hair of *lena* effectively. The texture components present in the table-mat and the clothes of *barbara* are also effectively restored. This is not visible in other cases where the texture profiles are smeared out and are not sharply visible. Further, the proposed algorithm is successful in restoring the sharp edges of the images of *lena* and *barbara* thereby improving to the total image quality.

In order to further justify the claims about the effectiveness of the proposed algorithm in restoring the textures and edges of an image simultaneously, an extensive study is carried out using the LIVE database [50] images as shown in Table 1. Here, the images are arranged in descending order of the texture (T) contributions. The corresponding image decomposition into texture (T), edge (E) and plain (P) of each individual image is given in percentage. Further the best value of group size K and fractional order α is also reported. All the images in LIVE database are subjected to Gauss blur of size $s = 11$ with varying additive white Gaussian noise of standard deviation (*SD*) 20 and 40. These images

FIGURE 12. Denoising results for the image *Lena* degraded due to Gauss blur (*G*) and Gaussian noise having standard deviation of 20 (a) Noisy image (b) **R-NL**, PSNR (SSIM) = 29.34(0.831); (c) **Cuesta**, PSNR (SSIM) = 27.04(0.753); (d) **Ada-Reg**, PSNR (SSIM) = 30.12(0.813); (e) **FTV-PA**, PSNR (SSIM) = 27.69(0.752); (f) **OLGS**, PSNR(SSIM) = 30.27(0.832); (g) **FFAD**, PSNR(SSIM) = 29.43(0.831) (h) **HF-OLGS**, PSNR(SSIM) = 31.12(0.874). (a) Noisy image.

FIGURE 13. Denoising results for the image *Barbara* degraded due to Gauss blur (*G*) and Gaussian noise having standard deviation of 30 (a) Noisy image (b) **R-NL**, PSNR (SSIM) = 28.96(0.761); (c) **Cuesta**, PSNR (SSIM) = 26.80(0.749); (d) **Ada-Reg**, PSNR (SSIM) = 28.78(0.731); (e) **FTV-PA**, PSNR (SSIM) = 25.31(0.753); (f) **OLGS**, PSNR(SSIM) = 29.31(0.841); (g) **FFAD**, PSNR(SSIM) = 27.92(0.776) (h) **HF-OLGS**, PSNR(SSIM) = 29.37(0.852). (a) Noisy image.

are restored using the seven different methods and the quality of the restored images is evaluated using image quality metrics such as PSNR and SSIM. It can be observed from the table that with images having varying texture and edge contributions, the proposed algorithm restores the image well in most of the cases. This observation is made based on the values reported in terms of PSNR(SSIM) scores in the table. In some case GMM produces good quality scores compared to our method. But when compared with other methods our method produces more pleasing and artifacts-free restored images.

Another important factor to measure the effectiveness of the denoising methods is run time. Table 2 shows the run time for various methods in case of Gaussian noise of standard deviation 40. It can be observed from the table that our proposed method is considerably faster than the other methods.

D. COMPARISON WITH DEEP LEARNING METHODS

Recently, deep learning based methods are gaining attention due to their remarkable denoising performance. Therefore, it is of interest to compare the performance of the

TABLE 1. Images are selected from LIVE database and categorized into Texture (T), Edge (E) and Plain (P) blocks. Arranged in decreasing order of their Texture (T) contribution. Denoising performance of the images subjected to Gaussian (*G*) blur with $s = 11$ and $\eta = 3.3$ for different noise levels (*SD*) is evaluated in terms of PSNR in dB (SSIM). The best group size K and fractional order α for each image is also reported.

								PSNR(SSIM)						
Images	**T(%)**	**E (%)**	**P(%)**	K	α	**Blur**	*SD*	**Cuesta** [38]	**FTV-PA** [60]	**R-NL** [61]	**Ada-Reg** [62]	**FFAD** [63]	**OLGS** [40]	**HF-OLGS**
stream	81.0	13.99	4.93	3	1.2	**G**	20	24.37 (0.752)	27.4 (0.773)	29.78 (0.830)	30.12 (0.823)	29.49 (0.836)	30.23 (0.826)	**31.21 (0.879)**
building2	66.3	30.23	3.45	3	1.2	**G**	20	23.89 (0.743)	28.38 (0.752)	29.45 (0.856)	30.18 (0.871)	28.12 (0.821)	30.47 (0.883)	**31.82 (0.923)**
studentsculpture	62.2	31.21	6.53	3	1.2	**G**	20	25.72 (0.759)	28.51 (0.768)	29.47 (0.822)	29.41 (0.812)	29.51 (0.843)	**29.55 (0.876)**	29.48 (0.874)
flowersonih35	55.5	19.07	25.41	3	1.2	**G**	20	26.16 (0.767)	28.52 (0.772)	29.50 (0.812)	29.43 (0.802)	29.59 (0.848)	29.62 (0.852)	**30.26 (0.857)**
sailing1	51.3	11.67	37.00	3	1.3	**G**	20	25.12 (0.749)	28.42 (0.758)	29.56 (0.821)	29.71 (0.813)	29.39 (0.841)	30.01 (0.835)	**30.13 (0.852)**
buildings	48.7	33.13	18.11	3	1.2	**G**	20	28.23 (0.743)	28.13 (0.749)	29.61 (0.843)	30.10 (0.872)	29.21 (0.834)	30.32 (0.881)	**31.52 (0.912)**
cemetry	47.7	31.89	20.36	3	1.4	**G**	20	28.17 (0.749)	27.43 (0.775)	29.52 (0.826)	29.86 (0.823)	29.27 (0.825)	30.19 (0.861)	**30.92 (0.864)**
rapids	44.4	31.36	24.21	3	1.2	**G**	40	26.80 (0.748)	25.32 (0.754)	28.97 (0.762)	28.78 (0.732)	27.92 (0.776)	**29.32 (0.842)**	29.26 (0.839)
woman	42.8	26.68	30.42	3	1.2	**G**	40	25.78 (0.741)	25.43 (0.762)	28.06 (0.723)	27.72 (0.751)	28.32 (0.821)	28.12 (0.768)	**28.52 (0.802)**
dancers	42.67	33.63	23.69	3	1.3	**G**	40	24.72 (0.687)	26.23 (0.751)	28.35 (0.826)	27.96 (0.793)	27.78 (0.787)	28.32 (0.716)	**28.84 (0.819)**
bikes	42.66	42.41	16.90	3	1.2	**G**	40	26.56 (0.736)	26.67 (0.769)	27.52 (0.778)	28.21 (0.841)	28.65 (0.834)	**28.64 (0.847)**	28.12 (0.785)
manfishing	40.67	30.04	27.29	3	1.2	**G**	40	25.72 (0.658)	26.32 (0.754)	27.47 (0.776)	28.82 (0.821)	28.24 (0.815)	29.06 (0.746)	28.32 (0.793)
paintedhouse	40.62	27.31	32.05	3	1.2	**G**	40	26.81 (0.750)	25.56 (0.764)	28.73 (0.816)	28.86 (0.862)	28.27 (0.825)	29.33 (0.821)	**30.34 (0.857)**
sailing4	38.92	17.73	44.28	3	1.2	**G**	40	26.67 (0.733)	26.12 (0.745)	28.67 (0.790)	28.78 (0.782)	28.25 (0.817)	29.21 (0.813)	**29.81 (0.847)**
lighthouse	37.98	16.13	44.93	3	1.3	**G**	20	26.42 (0.711)	27.76 (0.771)	27.82 (0.783)	28.21 (0.822)	28.57 (0.821)	28.71 (0.824)	**29.30 (0.839)**
house	36.76	19.87	43.42	3	1.2	**G**	20	26.71 (0.762)	28.46 (0.767)	29.21 (0.827)	29.50 (0.820)	29.43 (0.842)	29.89 (0.857)	**30.68 (0.865)**
ocean	36.70	13.05	50.18	3	1.4	**G**	20	26.22 (0.754)	28.15 (0.768)	29.22 (0.832)	29.45 (0.826)	29.11 (0.813)	30.25 (0.821)	**30.56 (0.852)**
churchandcapitol	34.22	27.83	37.94	3	1.2	**G**	20	26.31 (0.702)	28.56 (0.726)	29.63 (0.789)	29.85 (0.839)	29.23 (0.756)	30.52 (0.842)	**31.18 (0.872)**
coinsinfountain	32.09	42.69	25.21	3	1.2	**G**	20	26.17 (0.689)	28.28 (0.763)	29.42 (0.782)	29.28 (0.832)	29.42 (0.826)	30.41 (0.842)	**30.67 (0.865)**
lighthouse2	30.57	18.77	50.64	3	1.3	**G**	20	26.27 (0.729)	28.15 (0.742)	29.68 (0.820)	29.82 (0.848)	29.67 (0.787)	**30.42 (0.813)**	30.12 (0.821)
womanhat	24.08	19.73	56.17	3	1.2	**G**	20	26.21 (0.719)	28.76 (0.782)	29.55 (0.804)	30.31 (0.820)	30.24 (0.814)	30.56 (0.821)	**31.12 (0.869)**
plane	21.14	13.51	65.34	3	1.3	**G**	40	26.83 (0.751)	26.13 (0.771)	27.32 (0.785)	27.92 (0.823)	28.21 (0.834)	28.16 (0.807)	**28.62 (0.816)**
sailing3	16.99	25.45	57.54	3	1.2	**G**	40	26.79 (0.747)	26.23 (0.727)	28.34 (0.763)	28.35 (0.812)	28.34 (0.828)	**28.12 (0.790)**	27.91 (0.786)
sailing2	16.72	19.5	63.77	3	1.4	**G**	40	26.63 (0.731)	26.11 (0.739)	28.50 (0.802)	28.13 (0.802)	27.62 (0.779)	28.42 (0.801)	**28.56 (0.812)**
statue	16.17	30.89	52.92	3	1.2	**G**	40	25.74 (0.640)	25.31 (0.749)	27.37 (0.785)	28.36 (0.732)	27.82 (0.771)	27.72 (0.747)	**27.82 (0.772)**
caps	14.69	14.45	70.84	3	1.2	**G**	40	25.78 (0.642)	26.35 (0.717)	28.06 (0.767)	28.26 (0.803)	28.17 (0.823)	28.56 (0.825)	**29.26 (0.832)**
parrots	6.32	18.16	75.51	3	1.2	**G**	40	26.77 (0.746)	26.13 (0.748)	28.12 (0.874)	28.80 (0.802)	27.79 (0.789)	28.97 (0.821)	**29.11 (0.823)**
monarch	5.40	37.67	56.91	3	1.3	**G**	40	26.72 (0.737)	25.12 (0.702)	27.87 (0.802)	28.06 (0.836)	27.92 (0.779)	27.02 (0.719)	**27.56 (0.751)**

TABLE 2. Run time (in seconds) results of different denoising algorithms on LIVE dataset images degraded due to Gaussian noise with standard deviation (*SD*) of 40.

Noise standard deviation (SD)	Cuesta [38]	FTV-PA [60]	R-NL [61]	Ada-Reg [62]	FFAD [63]	OLGS [40]	HF-OLGS
40	7.82	7.43	4.32	11.23	6.24	3.43	2.3

proposed method with that of the recently introduced deep learning methods, namely DnCNN [67] and FFDNet [68]. These two denoising schemes are tested on LIVE dataset. The average PSNR(SSIM) values for Gaussian noise level (SD) of 40 are 29.16(0.833) for DnCNN and 29.32(0.837) for FFDNet. The corresponding values for our proposed work are 29.03(0.820). One can observe that the average PSNR(SSIM) of the proposed method are slightly lower than that of deep learning methods. But, the main advantage of using the proposed method is to preserve the texture present in an image. It is true that deep learning frameworks have provided good results, but in order to implement the deep nets, we need a huge database for their training. It should be noted that when we are dealing with two different kinds of noise, Gaussian and Poisson as done in this paper, the only modification that is required mathematically is the change in the data fidelity term whereas the regularizer term remains the same ((16) and (17)). However, if we have to carry out the same task via deep learning, we need twice the amount of data for training, i.e., one for each type of noise. Hence, in terms of time and computational resources needed to achieve denoising results, it is clear that the proposed mathematical optimization technique has advantages over deep learning technique

VI. CONCLUSION

A higher order fractional-based overlapping group sparsity (HF-OLGS) prior is introduced in this paper. It has been shown that the proposed HF-OLGS prior is capable of not only reducing the staircase effects present in the edges but also preserving the texture. The use of fractional derivatives in the optimization framework are solved using an efficient numerical scheme. In order to solve the image denoising framework formulated as a minimization problem, the energy function has been optimized using ADMM scheme. A detailed discussion about the parameter selection criteria needed to run the algorithm properly has been carried out. Restoration of images degraded by Gaussian or Poisson noise is considered in this paper. The restoration performance of the proposed denoising framework has been analysed on LIVE dataset which consists of images having varying texture, plain and edge contributions. Further, the optimal fractional order α and group size K for which the solution is feasible has also been provided for each image. The experimental results presented in this work show that with proper parameter settings, the algorithm yields good PSNR and SSIM scores comparable with that of the other methods. Moreover, the visual effects,

especially in high oscillatory regions (textures), are greatly improved.

Appendix A PROOF OF CONVEXITY OF THE ENERGY FUNCTION

We prove first the convexity for the case of Gaussian noise. Using (15) and (16), the energy function Z can be re-written for the Gaussian case as

$$Z(u) = (Hu - g)^2 + \beta_1[\phi(D^\alpha u)] + \beta_2[\phi(D_2^\alpha u)] \quad (42)$$

where

$$D_2^\alpha = \begin{bmatrix} D_{xx}^\alpha \\ D_{yy}^\alpha \\ D_{xy}^\alpha \\ D_{yx}^\alpha \end{bmatrix} \quad \text{and } D^\alpha = \begin{bmatrix} D_x^\alpha \\ D_y^\alpha \end{bmatrix}$$

Therefore, the convexity of Z in this case is assured if we establish

$$Z(tu + (1-t)v) \leq tZ(u) + (1-t)Z(v), \quad \forall\, 0 \leq t \leq 1$$

for any u and v. Letting u to $tu + (1-t)v$ in (42) , we get

$$\begin{aligned} Z(tu + (1-t)v) = \Big\{ & t^2(Hu - g)^2 + (1-t)^2(Hv - g)^2 \\ & +2t(1-t)(Hu - g)(Hv - f) \\ & \beta_1[\phi(D^\alpha(tu + (1-t)v))] \\ & \beta_2[\phi(D_2^\alpha(tu + (1-t)v))] \Big\} \end{aligned} \quad (43)$$

Using the fact that $\phi(A + B) \leq \phi(A) + \phi(B)$ results in

$$\begin{aligned} Z(tu + (1-t)v) \leq \Big\{ & t^2(Hu - g)^2 + (1-t)^2(Hv - g)^2 \\ & + t(1-t)\Big((Hu - g)^2 + (Hv - g)^2\Big) \\ & t\beta_1[\phi(D^\alpha u)] + (1-t)\beta_1[\phi(D^\alpha v)] \\ & t\beta_2[\phi(D_2^\alpha u)] + (1-t)\beta_2[\phi(D_2^\alpha v)] \Big\} \end{aligned} \quad (44)$$

A re-arrangement of the right side expression gives

$$\begin{aligned} & Z(tu + (1-t)v) \\ & \quad \leq \Big\{ t(Hu - g)^2 + t\beta_1[\phi(D^\alpha u)] \\ & \qquad + t\beta_2[\phi(D_2^\alpha u)] + (1-t)(Hv - g)^2 \\ & \qquad + (1-t)\beta_1[\phi(D^\alpha v)] + (1-t)\beta_2[\phi(D_2^\alpha v)] \Big\} \\ & \qquad \leq tZ(u) + (1-t)Z(v) \end{aligned} \quad (45)$$

This completes the proof for the Gaussian case.

Similarly, it can be shown that the energy function Z corresponding to the Poisson case is also convex.

REFERENCES

[1] R. Fergus, B. Singh, A. Hertzmann, S. T. Roweis, and W. T. Freeman, "Removing camera shake from a single photograph," *ACM Trans. Graph.*, vol. 25, no. 3, pp. 787–794, 2006.
[2] J.-F. Cai, H. Ji, C. Liu, and Z. Shen, "Blind motion deblurring from a single image using sparse approximation," in *Proc. IEEE Conf. Comput. Vis. Pattern Recognit. (CVPR)*, Jun. 2009, pp. 104–111.
[3] D. Krishnan and R. Fergus, "Fast image deconvolution using hyper-laplacian priors," in *Proc. Adv. Neural Inf. Process. Syst.*, 2009, pp. 1033–1041.
[4] D. Krishnan, T. Tay, and R. Fergus, "Blind deconvolution using a normalized sparsity measure," in *Proc. IEEE Conf. Comput. Vis. Pattern Recognit. (CVPR)*, Jun. 2011, pp. 233–240.
[5] L. I. Rudin, S. Osher, and E. Fatemi, "Nonlinear total variation based noise removal algorithms," *Phys. D, Nonlinear Phenomena*, vol. 60, nos. 1–4, pp. 259–268, 1992.
[6] T. Chan, A. Marquina, and P. Mulet, "High-order total variation-based image restoration," *SIAM J. Sci. Comput.*, vol. 22, no. 2, pp. 503–516, 2000.
[7] M. Lysaker and X.-C. Tai, "Iterative image restoration combining total variation minimization and a second-order functional," *Int. J. Comput. Vis.*, vol. 66, no. 1, pp. 5–18, 2006.
[8] K. Papafitsoros and C.-B. Schönlieb, "A combined first and second order variational approach for image reconstruction," *J. Math. Imag. Vis.*, vol. 48, no. 2, pp. 308–338, 2014.
[9] M. Lysaker, A. Lundervold, and X.-C. Tai, "Noise removal using fourth-order partial differential equation with applications to medical magnetic resonance images in space and time," *IEEE Trans. Image Process.*, vol. 12, no. 12, pp. 1579–1590, Dec. 2003.
[10] G. Gilboa and S. Osher, "Nonlocal operators with applications to image processing," *Multiscale Model. Simul.*, vol. 7, no. 3, pp. 1005–1028, 2008.
[11] J. Liu, T.-Z. Huang, Z. Xu, and X.-G. Lv, "High-order total variation-based multiplicative noise removal with spatially adapted parameter selection," *J. Opt. Soc. Amer. A, Opt. Image Sci., Vis.*, vol. 30, no. 10, pp. 1956–1966, 2013.
[12] W. Zhou and Q. Li, "Poisson noise removal scheme based on fourth-order PDE by alternating minimization algorithm," *Abstr. Appl. Anal.*, vol. 2012, Nov. 2012, Art. no. 965281.
[13] K. Bredies, K. Kunisch, and T. Pock, "Total generalized variation," *SIAM J. Imag. Sci.*, vol. 3, no. 3, pp. 492–526, 2010.
[14] X.-D. Wang, X.-C. Feng, W.-W. Wang, and W.-J. Zhang, "Iterative reweighted total generalized variation based Poisson noise removal model," *Appl. Math. Comput.*, vol. 223, pp. 264–277, Oct. 2013.
[15] Y. Shi, J. Song, and X. Hua, "Poissonian image deblurring method by non-local total variation and framelet regularization constraint," *Comput. Elect. Eng.*, vol. 62, pp. 319–329, Aug. 2016.
[16] G. Landi and E. L. Piccolomini, "An efficient method for nonnegatively constrained total variation-based denoising of medical images corrupted by Poisson noise," *Comput. Med. Imag. Graph.*, vol. 36, no. 1, pp. 38–46, 2012.
[17] S. Bonettini and V. Ruggiero, "On the convergence of primal–dual hybrid gradient algorithms for total variation image restoration," *J. Math. Imag. Vis.*, vol. 44, no. 3, pp. 236–253, 2012.
[18] D. Chen, Y. Chen, and D. Xue, "Fractional-order total variation image restoration based on primal-dual algorithm," *Abstr. Appl. Anal.*, vol. 2013, Sep. 2013, Art. no. 585310.
[19] J. Zhang, Z. Wei, and L. Xiao, "Adaptive fractional-order multi-scale method for image denoising," *J. Math. Imag. Vis.*, vol. 43, no. 1, pp. 39–49, 2012.
[20] Z. Jun and W. Zhihui, "A class of fractional-order multi-scale variational models and alternating projection algorithm for image denoising," *Appl. Math. Model.*, vol. 35, no. 5, pp. 2516–2528, 2011.
[21] Y. Zhang, Y. F. Pu, J. R. Hu, and J. L. Zhou, "A class of fractional-order variational image inpainting models," *Appl. Math. Inf. Sci.*, vol. 6, no. 2, pp. 299–306, 2012.
[22] Z. Ren, C. He, and Q. Zhang, "Fractional order total variation regularization for image super-resolution," *Signal Process.*, vol. 93, no. 9, pp. 2408–2421, 2013.
[23] J. Bai and X. C. Feng, "Fractional-order anisotropic diffusion for image denoising," *IEEE Trans. Image Process.*, vol. 16, no. 10, pp. 2492–2502, Oct. 2007.
[24] M. Ding, T.-Z. Huang, S. Wang, J.-J. Mei, and X.-L. Zhao, "Total variation with overlapping group sparsity for deblurring images under cauchy noise," *Appl. Math. Comput.*, vol. 341, pp. 128–147, Jan. 2019.

[25] X.-L. Zhao, F. Wang, and M. K. Ng, "A new convex optimization model for multiplicative noise and blur removal," *SIAM J. Imag. Sci.*, vol. 7, no. 1, pp. 456–475, 2014.
[26] Z. Gao *et al.*, "Motion tracking of the carotid artery wall from ultrasound image sequences: A nonlinear state-space approach," *IEEE Trans. Med. Imag.*, vol. 37, no. 1, pp. 273–283, Jan. 2018.
[27] Z. Gao *et al.*, "Robust estimation of carotid artery wall motion using the elasticity-based state-space approach," *Med. Image Anal.*, vol. 37, pp. 1–21, Apr. 2017.
[28] Z. Gao *et al.*, "Robust recovery of myocardial kinematics using dual H_∞ criteria," *Multimedia Tools Appl.*, vol. 77, no. 17, pp. 23043–23071, 2018.
[29] S. Parameswaran, C.-A. Deledalle, L. Denis, and T. Q. Nguyen, "Accelerating GMM-based patch priors for image restoration: Three ingredients for a 100× speed-up," *IEEE Trans. Image Process.*, vol. 28, no. 2, pp. 687–698, Feb. 2018.
[30] M. Gong, K. Zhang, T. Liu, D. Tao, C. Glymour, and B. Schölkopf, "Domain adaptation with conditional transferable components," in *Proc. Int. Conf. Mach. Learn.*, 2016, pp. 2839–2848.
[31] M. K. Ng, X. Yuan, and W. Zhang, "Coupled variational image decomposition and restoration model for blurred cartoon-plus-texture images with missing pixels," *IEEE Trans. Image Process.*, vol. 22, no. 6, pp. 2233–2246, Jun. 2013.
[32] S. Ono, T. Miyata, and I. Yamada, "Cartoon-texture image decomposition using blockwise low-rank texture characterization," *IEEE Trans. Image Process.*, vol. 23, no. 3, pp. 1128–1142, Mar. 2014.
[33] X. Liu, "A new TGV-Gabor model for cartoon-texture image decomposition," *IEEE Signal Process. Lett.*, vol. 25, no. 8, pp. 1221–1225, Aug. 2018.
[34] D.-Q. Chen and L.-Z. Cheng, "Deconvolving Poissonian images by a novel hybrid variational model," *J. Vis. Commun. Image Represent.*, vol. 22, no. 7, pp. 643–652, 2011.
[35] R. Chan, A. Lanza, S. Morigi, and F. Sgallari, "An adaptive strategy for the restoration of textured images using fractional order regularization," *Numer. Math., Theory, Methods Appl.*, vol. 6, no. 1, pp. 276–296, 2013.
[36] Y. Pu, "Fractional calculus approach to texture of digital image," in *Proc. 8th Int. Conf. Signal Process.*, vol. 2, Nov. 2006, pp. 1–5.
[37] P. U. Yi-Fei, "Fractional differential analysis for texture of digital image," *J. Algorithms Comput. Technol.*, vol. 1, no. 3, pp. 357–380, 2007.
[38] E. Cuesta, M. Kirane, and S. A. Malik, "Image structure preserving denoising using generalized fractional time integrals," *Signal Process.*, vol. 92, no. 2, pp. 553–563, 2012.
[39] Y. Wang, Y. Shao, Z. Gui, Q. Zhang, L. Yao, and Y. Liu, "A novel fractional-order differentiation model for low-dose CT image processing," *IEEE Access*, vol. 4, pp. 8487–8499, 2016.
[40] J. Liu, T.-Z. Huang, I. W. Selesnick, X.-G. Lv, and P.-Y. Chen, "Image restoration using total variation with overlapping group sparsity," *Inf. Sci.*, vol. 295, pp. 232–246, Feb. 2015.
[41] S. Boyd, N. Parikh, E. Chu, B. Peleato, and J. Eckstein, "Distributed optimization and statistical learning via the alternating direction method of multipliers," *Found. Trends Mach. Learn.*, vol. 3, no. 1, pp. 1–122, Jan. 2011.
[42] I. W. Selesnick and P.-Y. Chen, "Total variation denoising with overlapping group sparsity," in *Proc. IEEE Int. Conf. Acoust., Speech Signal Process. (ICASSP)*, May 2013, pp. 5696–5700.
[43] G. Peyré and J. Fadili, "Group sparsity with overlapping partition functions," in *Proc. 19th Eur. Signal Process. Conf.*, Aug. 2011, pp. 303–307.
[44] M. Figueiredo and J. Bioucas-Dias, "An alternating direction algorithm for (overlapping) group regularization," *Signal Process. Adapt. Sparse Struct. Represent.*, 2011.
[45] J. Zhang, Z. Wei, and L. Xiao, "A fast adaptive reweighted residual-feedback iterative algorithm for fractional-order total variation regularized multiplicative noise removal of partly-textured images," *Signal Process.*, vol. 98, pp. 381–395, May 2014.
[46] M. R. Hestenes, "Multiplier and gradient methods," *J. Optim. Theory Appl.*, vol. 4, no. 5, pp. 303–320, 1969.
[47] D. R. Hunter and K. Lange, "A tutorial on MM algorithms," *Amer. Statist.*, vol. 58, no. 1, pp. 30–37, 2004.
[48] M. A. T. Figueiredo, J. M. Bioucas-Dias, and R. D. Nowak, "Majorization–minimization algorithms for wavelet-based image restoration," *IEEE Trans. Image Process.*, vol. 16, no. 12, pp. 2980–2991, Dec. 2007.
[49] M. R. Hestenes and E. Stiefel, *Methods of Conjugate Gradients for Solving Linear Systems*, vol. 49, no. 1. Washington, DC, USA: NBS, 1952.
[50] H. R. Sheikh, Z. Wang, L. Cormack, and A. C. Bovik. (2016). *LIVE Image Quality Assessment Database Release 2*. [Online]. Available: http://live.ece.utexas.edu/research/quality
[51] Z. Wang, A. C. Bovik, H. R. Sheikh, and E. P. Simoncelli, "Image quality assessment: From error visibility to structural similarity," *IEEE Trans. Image Process.*, vol. 13, no. 4, pp. 600–612, Apr. 2004.
[52] X. K. Yang, W. S. Ling, Z. K. Lu, E. P. Ong, and S. S. Yao, "Just noticeable distortion model and its applications in video coding," *Signal Process., Image Commun.*, vol. 20, no. 7, pp. 662–680, Aug. 2005.
[53] X. H. Zhang, W. S. Lin, and P. Xue, "Improved estimation for just-noticeable visual distortion," *Signal Process.*, vol. 85, no. 4, pp. 795–808, 2005.
[54] X. Zhang, W. Lin, and P. Xue, "Just-noticeable difference estimation with pixels in images," *J. Vis. Commun. Image Represent.*, vol. 19, no. 1, pp. 30–41, Jan. 2008.
[55] Z. Wei and K. N. Ngan, "Spatio-temporal just noticeable distortion profile for grey scale image/video in DCT domain," *IEEE Trans. Circuits Syst. Video Technol.*, vol. 19, no. 3, pp. 337–346, Mar. 2009.
[56] A. Liu, W. Lin, M. Paul, C. Deng, and F. Zhang, "Just noticeable difference for images with decomposition model for separating edge and textured regions," *IEEE Trans. Circuits Syst. Video Technol.*, vol. 20, no. 11, pp. 1648–1652, Nov. 2010.
[57] D. Chen, Y. Chen, and D. Xue, "Fractional-order total variation image denoising based on proximity algorithm," *Appl. Math. Comput.*, vol. 257, pp. 537–545, Apr. 2015.
[58] C. Sutour, C.-A. Deledalle, and J.-F. Aujol, "Adaptive regularization of the NL-means: Application to image and video denoising," *IEEE Trans. Image Process.*, vol. 23, no. 8, pp. 3506–3521, Aug. 2014.
[59] V. Estellers, S. Soatto, and X. Bresson, "Adaptive regularization with the structure tensor," *IEEE Trans. Image Process.*, vol. 24, no. 6, pp. 1777–1790, Jun. 2015.
[60] M. Janev, S. Pilipović, T. Atanacković, R. Obradović, and N. Ralević, "Fully fractional anisotropic diffusion for image denoising," *Math. Comput. Model.*, vol. 54, no. 1, pp. 729–741, 2011.
[61] S. Tao, W. Dong, Z. Xu, and Z. Tang, "Fast total variation deconvolution for blurred image contaminated by Poisson noise," *J. Vis. Commun. Image Represent.*, vol. 38, pp. 582–594, Jul. 2016.
[62] X.-G. Lv, L. Jiang, and J. Liu, "Deblurring Poisson noisy images by total variation with overlapping group sparsity," *Appl. Math. Comput.*, vol. 289, pp. 132–148, Oct. 2016.
[63] H. Fang, L. Yan, H. Liu, and Y. Chang, "Blind Poissonian images deconvolution with framelet regularization," *Opt. Lett.*, vol. 38, no. 4, pp. 389–391, 2013.
[64] L. Yan, H. Fang, and S. Zhong, "Blind image deconvolution with spatially adaptive total variation regularization," *Opt. Lett.*, vol. 37, no. 14, pp. 2778–2780, 2012.
[65] X. Gong, B. Lai, and Z. Xiang, "A L_0 sparse analysis prior for blind Poissonian image deconvolution," *Opt. Express*, vol. 22, no. 4, pp. 3860–3865, 2014.
[66] J. G. Nagy, K. Palmer, and L. Perrone, "Iterative methods for image deblurring: A MATLAB object-oriented approach," *Numer. Algorithms*, vol. 36, no. 1, pp. 73–93, 2004.
[67] K. Zhang, W. Zuo, Y. Chen, D. Meng, and L. Zhang, "Beyond a Gaussian Denoiser: Residual learning of deep CNN for image denoising," *IEEE Trans. Image Process.*, vol. 26, no. 7, pp. 3142–3155, Jul. 2017.
[68] K. Zhang, W. Zuo, and L. Zhang, "FFDNet: Toward a fast and flexible solution for CNN-based image denoising," *IEEE Trans. Image Process.*, vol. 27, no. 9, pp. 4608–4622, Sep. 2018.

AHLAD KUMAR received the B.Tech. degree in electronics and communication engineering from Jamia Millia Islamia, India, in 2005, the M.Tech. degree from ABV-IIITM, in 2005, and the Ph.D. degree from the University of Malaya, in 2016. He is currently a Postdoctoral Fellow with Concordia University, Montreal, Canada. He has published several papers in international journals. His research interests include image denoising, low voltage analog, and mixed signal design. He has served as a Reviewer for several international journals and conferences.

M. OMAIR AHMAD (S'69–M'78–SM'83–F'01) received the B.Eng. degree in electrical engineering from Sir George Williams University, Montreal, QC, Canada, and the Ph.D. degree in electrical engineering from Concordia University, Montreal. From 1978 to 1979, he was a Faculty Member with the New York University College, Buffalo, NY, USA. In 1979, he joined the Faculty of Concordia University as an Assistant Professor of computer science. Subsequently, he joined the Department of Electrical and Computer Engineering, Concordia University, where he was the Chair of the Department, from 2002 to 2005, where he is currently a Professor. He was a Founding Researcher of Micronet, a Canadian Network of Centers of Excellence, from 1990 to 2004. He was a Guest Professor with Southeast University, Nanjing, China. He is also the Concordia University Research Chair (Tier I) in multimedia signal processing. He has authored in signal processing and holds four patents. His current research interests include image and speech processing, biomedical signal processing, watermarking, biometrics, video signal processing, object detection and tracking, deep learning techniques in signal processing, and fast signal transforms and algorithms. In 1988, he was a member of the Admission and Advancement Committee of the IEEE. He was a recipient of numerous honors and awards, including the Wighton Fellowship from the Sandford Fleming Foundation, an induction to Provosts Circle of Distinction for Career Achievements, and the Award of Excellence in Doctoral Supervision from the Faculty of Engineering and Computer Science, Concordia University. He was the Local Arrangements Chairman of the 1984 IEEE International Symposium on Circuits and Systems. He has served as the Program Co-Chair for the 1995 IEEE International Conference on Neural Networks and Signal Processing, the 2003 IEEE International Conference on Neural Networks and Signal Processing, and the 2004 IEEE International Midwest Symposium on Circuits and Systems. He was the General Co-Chair of the 2008 IEEE International Conference on Neural Networks and Signal Processing. He is the Chair of the Montreal Chapter IEEE Circuits and Systems Society. He was an Associate Editor of the IEEE TRANSACTIONS ON CIRCUITS AND SYSTEMS Part I: FUNDAMENTAL THEORY AND APPLICATIONS, from 1999 to 2001.

M. N. S. SWAMY (S'59–M'62–SM'74–F'80) received the B.Sc. degree (Hons.) in mathematics from the University of Mysore, Mysore, India, in 1954, the Diploma degree in electrical communication engineering from the Indian Institute of Science, Bengaluru, India, in 1957, and the M.Sc. and Ph.D. degrees in electrical engineering from the University of Saskatchewan, Saskatoon, SK, Canada, in 1960 and 1963, respectively. He was conferred with the title of Honorary Professor by National Chiao Tong University, Hsinchu, Taiwan, in 2009. He is currently a Research Professor with the Department of Electrical and Computer Engineering, Concordia University, Montreal, QC, Canada, where he served as the Founding Chair of the Department of Electrical Engineering, from 1970 to 1977, and the Dean of Engineering and Computer Science, from 1977 to 1993. During that time, he developed the faculty into a research oriented one, from what was primarily an undergraduate faculty. Since 2001, he has been the Concordia Chair (Tier I) in signal processing. He has also taught at the Department of Electrical Engineering, Technical University of Nova Scotia, Halifax, NS, Canada, the University of Calgary, Calgary, AB, Canada, and the Department of Mathematics, University of Saskatchewan. He has published in number theory, circuits, systems, and signal processing, and holds five patents. He has co-authored nine books and five book chapters. He was a Founding Member of Micronet, a Canadian Network of Centers of Excellence, from 1990 to 2004, and also a Coordinator of Concordia University. He is a fellow of the Institute of Electrical Engineers, U.K., the Engineering Institute of Canada, the Institution of Engineers, India, and the Institution of Electronic and Telecommunication Engineers, India. He was inducted to the Provosts Circle of Distinction for career achievements, in 2009. He was a recipient of many IEEE-CAS Society awards, including, 1986, Guillemin-Cauer Best Paper Award, the Education Award, in 2000, and the Golden Jubilee Medal, in 2000. He has served as the Program Chair for, 1973, IEEE Circuits and Systems (CAS) Symposium, the General Chair for, 1984, IEEE CAS Symposium, the Vice Chair of, 1999, IEEE CAS Symposium, and a member of the Board of Governors of the CAS Society. He has been the Editor-in-Chief of the *Journal Circuits, Systems and Signal Processing* (CSSP), since 1999. Recently, CSSP has instituted the Best Paper Award in his name. He has served as the Editor-in-Chief for the IEEE TRANSACTIONS ON CIRCUITS AND SYSTEMS I, from 1999 to 2001, and an Associate Editor for the IEEE TRANSACTIONS ON CIRCUITS AND SYSTEMS, from 1985 to 1987. He has served the IEEE in various capacities, such as the President Elect, in 2003, the President, in 2004, the Past President, in 2005, the Vice President (publications), from 2001 to 2002, and the Vice President, in 1976.